We are IntechOpen, the world's leading publisher of Open Access books Built by scientists, for scientists

4,800
Open access books available

122,000
International authors and editors

135M
Downloads

Our authors are among the

154
Countries delivered to

TOP 1%
most cited scientists

12.2%
Contributors from top 500 universities

CLARIVATE ANALYTICS BOOK CITATION INDEX INDEXED

WEB OF SCIENCE™

Selection of our books indexed in the Book Citation Index in Web of Science™ Core Collection (BKCI)

Interested in publishing with us?
Contact book.department@intechopen.com

Numbers displayed above are based on latest data collected.
For more information visit www.intechopen.com

11

Theory of Unitary Spin Rotation and Spin State Tomography for a Single Electron and Two Electrons

T. Takagahara
Department of Electronics and Information Science,
Kyoto Institute of Technology, Matsugasaki, Kyoto 606-8585
CREST, Japan Science and Technology Agency,
4-1-8 Honcho, Kawaguchi, Saitama 332-0012,
Japan

1. Introduction

Coherent control of quantum states is a critical step toward many novel technological applications ranging from manipulation of quantum bits (qubits) in quantum logic gates to controlling the spin degrees of freedom of electrons [1–13]. A qubit with a longer coherence time is desirable for the application to the quantum information processing. Electron spins in semiconductor nanostructures are considered as one of the most promising candidates of the building blocks for quantum information processing due to their robustness against decoherence effects [14–18]. A quantum media converter between a photon qubit and an electron spin qubit was proposed for the use in quantum repeaters [19–22]. Quantum information can take several different forms and it is preferable to be able to convert among different forms. One form is the photon polarization and another is the electron spin polarization. Photons are the most convenient medium for sharing quantum information between distant locations. Electrons are the most efficient medium for manipulating the quantum information by electrical and optical means. The fundamental operations are the initialization, unitary rotation and measurement of a qubit. The initialization of a single electron spin was demonstrated by the efficient optical method [23–25]. Also, the coherent rotation of a single electron spin has been realized by the microwave ESR (Electron Spin Resonance) method [26] and by the optical STIRAP (STImulated Raman Adiabatic Passage) method with coherence times up to several μs [27–33] in III-V semiconductor nanostructures and up to several tens of ms in the localized electron systems in IV elemental semiconductors [34–36]. The optical STIRAP method is advantageous because of its ultrafast operation. However, the precise control of the spin rotation without leaving behind any population in the intermediate excited states has not yet been realized. It is also important to achieve the unitary spin rotation of two electrons, because the singlet-triplet subspace of two electrons was utilized as a qubit space and the electrical manipulation of the qubit was realized [16]. At the same time, it is absolutely necessary to confirm the quantum state of the electron after the spin state manipulation or the quantum state transfer from a photon, namely, to examine whether the electron spin is prepared in the desired state or not. This

Source: Advances in Lasers and Electro Optics, Book edited by: Nelson Costa and Adolfo Cartaxo,
ISBN 978-953-307-088-9, pp. 838, April 2010, INTECH, Croatia, downloaded from SCIYO.COM

requires the full state tomography, namely the measurement of the density matrix of the electron. This state tomography is also important to estimate the fidelity of relevant quantum operations.
Thus it is a challenging task to establish the precise spin rotation and the spin state tomography for both cases of a single electron and two electrons. We review the general aspects of the unitary spin rotation of a single electron by the STIRAP method and develop the scheme to rotate the pseudo-spin formed by the singlet state and the triplet states of two electrons based on the optical STIRAP process, discussing the optimal conditions for the precise control. Also we propose and analyze optical methods to achieve the electron spin state tomography based on the Faraday/Kerr rotation, referring to the recent experiments [37, 38].

2. Optical STIRAP method for spin rotation of a single electron

As mentioned in the Introduction, the spin rotation of a single electron is a crutial ingredient in the quantum information processing. It is desirable to accomplish the spin rotation along an arbitrary direction for an arbitrary rotation angle in a single-shot process. So far, the spin rotation of a single electron was demonstrated by optical and electrical means in the proofof- principle experiments. With respect to the required time for the spin rotation, the optical method based on the STIRAP (stimulated Raman adiabatic passage) process is preferable because of its ultrafast response. But the precise control of the spin rotation is yet to be pursued. Here several characteristics of this STIRAP process will be investigated.

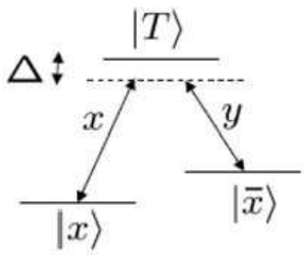

Fig. 1. Schematic energy level structure for the STIRAP process. Allowed optical transitions are depicted by x and y, which represent the mutually orthogonal polarizations. Δ denotes the off-resonance energy of the excitation lights relative to the transition energies. The Raman condition for the excitation lights is imposed.

In order to carry out the STIRAP process, a Λ-type transtion is necessary, as depicted in Fig. 1. The lowest two levels denoted by $|x\rangle$ and $|\bar{x}\rangle$ are the ground doublet states with close energies, e.g., the spin up and spin down states of a single electron or the ground and excited vibrational states of a single molecule. A pseudospin is composed of these doublet states and can be rotated by optical transitions via the intermediate excited state denoted by $|T\rangle$. The important point is that the selection rules of the left and right optical transitions are orthogonal to each other, which are depicted typically as x and y in Fig. 1. The doublet states are not directly connected optically. Then the relevant Hamiltonian is written as

$$H = H_0 + V \ , \tag{1}$$

$$H_0 = E_x|x\rangle\langle x| + E_{\bar{x}}|\bar{x}\rangle\langle\bar{x}| + E_T|T\rangle\langle T| \ , \tag{2}$$

$$\begin{aligned} V = &-\hbar\Omega_x(t)[e^{-i\omega_x t}|T\rangle\langle x| + e^{i\omega_x t}|x\rangle\langle T|] \\ &-\hbar\Omega_y(t)[e^{-i\omega_y t - i\delta}|T\rangle\langle\bar{x}| + e^{i\omega_y t + i\delta}|\bar{x}\rangle\langle T|] \ , \end{aligned} \tag{3}$$

where H_0 represents the unperturbed part, V the optical transitions, Ω_x and Ω_y the Rabi frequencies, δ the relative phase shift of the y-polarized light and the energy E_x is put as E_x = 0 for the origin of energy. Then the time evolution proceeds as follows:

$$i\hbar\dot{\psi} = H\psi \ , \ \psi = c_x|x\rangle + c_{\bar{x}}|\bar{x}\rangle + c_T|T\rangle \ , \tag{4}$$

$$\frac{d}{dt}\begin{pmatrix} c_x \\ c_{\bar{x}} \\ c_T \end{pmatrix} = \begin{pmatrix} i\Omega_x(t)e^{i\omega_x t}c_T \\ -i\frac{E_{\bar{x}}}{\hbar}c_{\bar{x}} + i\Omega_y(t)e^{i\omega_y t + i\delta}c_T \\ -i\frac{E_T}{\hbar}c_T + i\Omega_x(t)e^{-i\omega_x t}c_x + i\Omega_y(t)e^{-i\omega_y t - i\delta}c_{\bar{x}} \end{pmatrix} . \tag{5}$$

In order to single out the rapidly oscillating part, we put as

$$c_{\bar{x}}(t) = e^{-i\frac{E_{\bar{x}}}{\hbar}t}\tilde{c}_{\bar{x}}(t) \ , \ c_T(t) = e^{-i\frac{E_T}{\hbar}t}\tilde{c}_T(t) \ , \tag{6}$$

obtaining

$$\frac{d}{dt}\begin{pmatrix} c_x \\ \tilde{c}_{\bar{x}} \\ \tilde{c}_T \end{pmatrix} = \begin{pmatrix} i\Omega_x(t)e^{i(\omega_x - \frac{E_T}{\hbar})t}\tilde{c}_T \\ i\Omega_y(t)e^{i(\omega_y - \frac{E_T}{\hbar} + \frac{E_{\bar{x}}}{\hbar})t + i\delta}\tilde{c}_T \\ i\Omega_x(t)e^{-i(\omega_x - \frac{E_T}{\hbar})t}c_x + i\Omega_y(t)e^{-i(\omega_y - \frac{E_T}{\hbar} + \frac{E_{\bar{x}}}{\hbar})t - i\delta}\tilde{c}_{\bar{x}} \end{pmatrix} . \tag{7}$$

Now we postulate the Raman condition for the x and y polarized lights:

$$\frac{E_T}{\hbar} - \omega_x = \frac{E_T}{\hbar} - \frac{E_{\bar{x}}}{\hbar} - \omega_y = \Delta \tag{8}$$

and also assume the same pulse shape for the x- and y-polatized lights with arbitrary relative intensity ratio determined by θ:

$$\Omega_x(t) = \Omega_0(t)\cos\theta \ , \ \Omega_y(t) = \Omega_0(t)\sin\theta \ . \tag{9}$$

Introducing the bright and dark state amplitudes defined by

$$\begin{pmatrix} c_B \\ c_D \end{pmatrix} = \begin{pmatrix} \cos\theta & e^{-i\delta}\sin\theta \\ -e^{i\delta}\sin\theta & \cos\theta \end{pmatrix}\begin{pmatrix} c_x \\ \tilde{c}_{\bar{x}} \end{pmatrix} = U\begin{pmatrix} c_x \\ \tilde{c}_{\bar{x}} \end{pmatrix} \ , \tag{10}$$

we can simplify the equations of motion as

$$\frac{d}{dt}\begin{pmatrix} c_B \\ \tilde{c}_T \end{pmatrix} = \begin{pmatrix} i\Omega_0(t)e^{-i\Delta t}\,\tilde{c}_T \\ i\Omega_0(t)e^{i\Delta t}\,c_B \end{pmatrix} \ , \ \frac{d}{dt}c_D = 0 \ . \tag{11}$$

Thus the dark state does not change. The amplitudes of the bright state and the $|T\rangle$ state satisfy the following equations:

$$\frac{d^2}{dt^2}c_B = \left(\frac{\dot{\Omega}_0(t)}{\Omega_0(t)} - i\Delta\right)\frac{d}{dt}c_B - \Omega_0^2(t)c_B \ , \tag{12}$$

$$\frac{d^2}{dt^2}\tilde{c}_T = \left(\frac{\dot{\Omega}_0(t)}{\Omega_0(t)} + i\Delta\right)\frac{d}{dt}\tilde{c}_T - \Omega_0^2(t)\tilde{c}_T \ . \tag{13}$$

To develop the analytical solutions of these equations [39, 40], we assume a sech pulse envelope:

$$\Omega_0(t) = \Omega \ \mathrm{sech}(\sigma t) \ . \tag{14}$$

Introducing a dimensionless time variable by

$$\zeta = \frac{1}{2}(1 + \tanh(\sigma t)) \ , \tag{15}$$

we have

$$\zeta(1-\zeta)\frac{d^2}{d\zeta^2}c_B + \left(\frac{1}{2}(1 + i\frac{\Delta}{\sigma}) - \zeta\right)\frac{d}{d\zeta}c_B + \frac{\Omega^2}{\sigma^2}c_B = 0 \ , \tag{16}$$

$$\zeta(1-\zeta)\frac{d^2}{d\zeta^2}\tilde{c}_T + \left(\frac{1}{2}(1 - i\frac{\Delta}{\sigma}) - \zeta\right)\frac{d}{d\zeta}\tilde{c}_T + \frac{\Omega^2}{\sigma^2}\tilde{c}_T = 0 \ . \tag{17}$$

This is a hypergeometric differential equation. General solutions are given by

$$\begin{pmatrix} c_B(t) \\ \tilde{c}_T(t) \end{pmatrix} = \begin{pmatrix} F(\alpha, -\alpha, \gamma|\zeta) & e^{i\Delta t}\ \frac{i\alpha}{\gamma^*}\ \zeta^{\gamma^*} F(\alpha+\gamma^*, -\alpha+\gamma^*, 1+\gamma^*|\zeta) \\ e^{-i\Delta t}\ \frac{i\alpha}{\gamma}\ \zeta^{\gamma} F(\alpha+\gamma, -\alpha+\gamma, 1+\gamma|\zeta) & F(\alpha, -\alpha, \gamma^*|\zeta) \end{pmatrix} \times \begin{pmatrix} c_B(-\infty) \\ \tilde{c}_T(-\infty) \end{pmatrix} \tag{18}$$

$$\text{with} \quad \alpha = \frac{\Omega}{\sigma} \ , \ \beta = -\frac{\Omega}{\sigma} \ , \ \gamma = \frac{1}{2}(1 + i\frac{\Delta}{\sigma}) \ , \tag{19}$$

where $F(\alpha, \beta, \gamma|\zeta)$ is the hypergeometric function. In the rotation of the pseudospin, we start with the initial state in which

$$c_B(-\infty) = \text{finite} \ , \ c_D(-\infty) = \text{finite} \ , \ \tilde{c}_T(-\infty) = 0 \tag{20}$$

and after the pulse we prefer to have

$$\tilde{c}_T(\infty) = 0 \tag{21}$$

in order to leave no excitation in the intermediate excited state $|T\rangle$. To satisfy this condition, we should have

$$\frac{\alpha}{\gamma} F(\alpha+\gamma, -\alpha+\gamma, 1+\gamma|1) = 0 \tag{22}$$

because the asymptotic behavior ($t\to\infty$) is given by putting as $\zeta = 1$. Using the formula [41]

$$F(a,b,c|1) = \frac{\Gamma(c)\Gamma(c-a-b)}{\Gamma(c-a)\Gamma(c-b)} \tag{23}$$

which is valid under the condition that $\mathrm{Re}(c-a-b) > 0$ and $c \neq 0, -1, -2, \ldots$, we have

$$\frac{\alpha}{\gamma} F(\alpha+\gamma, -\alpha+\gamma, 1+\gamma|1) = \frac{\alpha}{\gamma} \frac{\Gamma(1+\gamma)\Gamma(1-\gamma)}{\Gamma(1-\alpha)\Gamma(1+\alpha)} \,. \tag{24}$$

Further, using the formulas

$$x\Gamma(x) = \Gamma(x+1) \,, \quad \Gamma(x)\Gamma(1-x) = \frac{\pi}{\sin \pi x} \,, \tag{25}$$

we obtain

$$\frac{\alpha}{\gamma} \frac{\Gamma(1+\gamma)\Gamma(1-\gamma)}{\Gamma(1-\alpha)\Gamma(1+\alpha)} = \frac{\alpha}{\gamma} \frac{\gamma\Gamma(\gamma)\Gamma(1-\gamma)}{\Gamma(1-\alpha)\alpha\Gamma(\alpha)} = \frac{\sin \pi\alpha}{\sin \pi\gamma} \,. \tag{26}$$

Putting in the expression of γ, we finally have

$$\frac{\alpha}{\gamma} F(\alpha+\gamma, -\alpha+\gamma, 1+\gamma|1) = \mathrm{sech}\left(\frac{\pi\Delta}{2\sigma}\right) \sin \pi\alpha \,. \tag{27}$$

This quantity vanishes only when α = 1, 2, … . This condition is nothing but the condition that the pulse area is 2π, 4π, … . This is quite reasonable because the Bloch vector rotates and returns to the initial state for the pulse area of integer times 2π.
Furthermore, under this condition, the amplitude of the bright state receives after a pulse an additional factor given by

$$F(\alpha, -\alpha, \gamma|1) = -\frac{\gamma^*}{\gamma} \,, \; \frac{\gamma^*(\gamma^*+1)}{\gamma(\gamma+1)} \,, \; -\frac{\gamma^*(\gamma^*+1)(\gamma^*+2)}{\gamma(\gamma+1)(\gamma+2)} \cdots \,, \tag{28}$$

where the expressions on the right hand side correspond to α = 1, 2, 3, … , respectively and their absolute magnitude is obviously unity and thus they can be put as

$$F(\alpha, -\alpha, \gamma|1) = e^{-i\phi} \,. \tag{29}$$

This phase ϕ determines the rotation angle of the pseudospin, as will be shown shortly. Now the effect of the pulse can be summarized as

$$\begin{pmatrix} c_B(\infty) \\ c_D(\infty) \end{pmatrix} = \begin{pmatrix} e^{-i\phi} & 0 \\ 0 & 1 \end{pmatrix} \begin{pmatrix} c_B(-\infty) \\ c_D(-\infty) \end{pmatrix} . \tag{30}$$

This relation can be rewritten in terms of $(c_x, \tilde{c}_{\bar{x}})$ amplitudes:

$$\begin{pmatrix} c_x(\infty) \\ \tilde{c}_{\bar{x}}(\infty) \end{pmatrix} = U^\dagger \begin{pmatrix} e^{-i\phi} & 0 \\ 0 & 1 \end{pmatrix} U \begin{pmatrix} c_x(-\infty) \\ \tilde{c}_{\bar{x}}(-\infty) \end{pmatrix} , \tag{31}$$

where the operation of the pulse is calculated as

$$\begin{aligned} U^\dagger \begin{pmatrix} e^{-i\phi} & 0 \\ 0 & 1 \end{pmatrix} U &= e^{-i\phi/2} \left[\cos\frac{\phi}{2} \overleftrightarrow{\mathbf{1}} - i \sin\frac{\phi}{2} \, (\vec{n} \cdot \vec{\sigma}) \right] = e^{-i\phi/2} \, \exp\left[-i\frac{\phi}{2} \, \vec{n} \cdot \vec{\sigma} \right] \\ &= e^{-i\phi/2} \, \exp\left[-i\phi \, \vec{n} \cdot \vec{S} \right] \end{aligned} \tag{32}$$

$$\text{with} \quad \vec{n} = (\sin 2\theta \cos\delta, \sin 2\theta \sin\delta, \cos 2\theta) , \quad \tan\theta = \frac{\Omega_y}{\Omega_x} . \tag{33}$$

This relation indicates that the pseudospin vector composed of $|x\rangle$ and $|\bar{x}\rangle$ states is rotated by an angle ϕ around the direction vector $\vec{n}$. The rotation angle ϕ can be tuned by the off-resonance energy Δ in Eq. (8), whereas the direction vector $\vec{n}$ can be adjusted by the intensity ratio and the relative phase shift between the orthogonally polarized lights with the same temporal envelope.

In order to estimate the fidelity of this spin rotation, we prepare an arbitrary initial state, follow the time evolution to obtain the asymptotic state, calculate the overlap with the ideal state and average over the initial states. In order to take into account relaxation processes, we consider the density matrix for the system composed of three states. We prepare an initial state:

$$\rho(-\infty) = |\psi(-\infty)\rangle\langle\psi(-\infty)| , \tag{34}$$

$$\psi(-\infty) = c_x(-\infty)|x\rangle + c_{\bar{x}}(-\infty)|\bar{x}\rangle \tag{35}$$

$$\text{with} \qquad \begin{pmatrix} c_x(-\infty) \\ c_{\bar{x}}(-\infty) \end{pmatrix} = \begin{pmatrix} \cos\theta_i/2 \; e^{-i\varphi_i/2} \\ \sin\theta_i/2 \; e^{i\varphi_i/2} \end{pmatrix} , \tag{36}$$

where θ_i and φ_i indicate the initial direction of the pseudospin. The time evolution of the density matrix is given by

$$\dot{\rho}(t) = -\frac{i}{\hbar}[H_0 + V, \rho] + \Gamma\rho , \tag{37}$$

where ¡ includes the population relaxation and decoherence terms. After the time evolution we have the asymptotic state $\pi(\infty)$, which is actually $\pi(T_f)$ for a large enough time T_f, and calculate the fidelity defined by the overlap of the actual density matrix with the ideal density matrix which is obtained without any relaxation terms:

$$F = \langle \mathrm{Tr}_{|x\rangle,|\bar{x}\rangle} \; \rho_{\mathrm{ideal}}(\infty)\rho(\infty) \rangle_{c_x, c_{\bar{x}}} , \tag{38}$$

where the angular bracket means the average over the initial spin direction, namely:

$$\langle \cdots \rangle_{c_x, c_{\bar{x}}} = \frac{1}{4\pi} \int_0^{\pi} d\theta_i \sin\theta_i \int_0^{2\pi} d\varphi_i \cdots . \tag{39}$$

Some numerical results will be presented for the fidelity and the residual population in the excited state $|T\rangle$. Because of the energy-time duality the following results can be applied for an arbitrary pulse width by scaling appropriately the off-resonance energy. But, for the definiteness, the optical pulse is assumed as sech (t/t_p) with t_p = 5ps and the time evolution is integrated over the time range of $-6t_p \le t \le 6t_p$. The relaxation parameters are chosen as

$$\hbar\Gamma_{T\to x} = \hbar\Gamma_{T\to\bar{x}} = 0.01\text{meV} \ , \ \hbar\gamma_{T\,x} = \hbar\gamma_{T\,\bar{x}} = 0.05\text{meV} \ , \tag{40}$$

where $\Gamma(\gamma)$ indicates the population relaxation (decoherence) rate. The equations of motion for the density matrix elements are similar to those given from Eq. (58) to Eq. (64) in the later section. First of all, the rotation angle ϕ is plotted in Fig. 2 as a function of the off-resonance energy. The normalized off-resonance energy is defined by Δt_p, where Δ is given in Eq. (8), and is dimensionless. For the 2π pulse the rotation angle is monotonically increasing with increasing off-resonance. The fidelity of the spin rotation is exhibited in Fig. 3. The fidelity is improved with increasing off-resonance in general for the 2π and 4π pulses. For the 6π pulse, a strange behavior is seen. But it can be understood that a fidelity peak appears around the off-resonance energy where the rotation angle is almost 360 degrees, namely, the spin returns to the initial state and the deviation from the ideal time evolution is suppressed. Another important quantity is the residual population in the excited state $|T\rangle$ and is exhibited in Fig. 4. This is monotonically decreasing with increasing off-resonance.

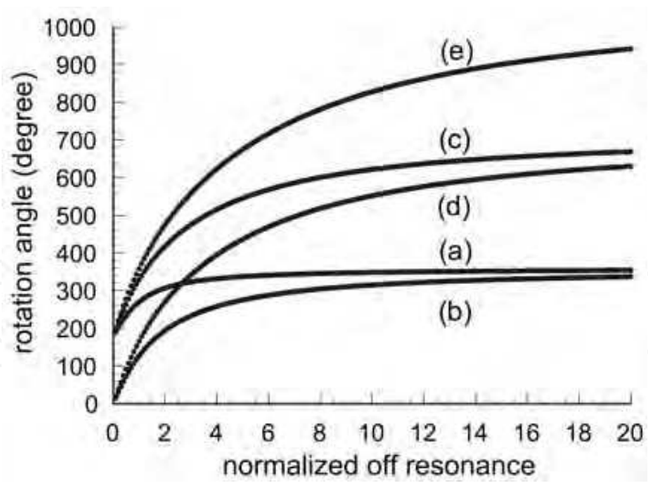

Fig. 2. Angles of the spin rotation are plotted as a function of the normalized off-resonance energy Δt_p for the pulse areas of (a) 2π, (b) 4π, (c) 6π, (d) 8π, and (e) 10π.

Analytically exact solutions are possible only for the sech pulses. In order to see the effect of the pulse shape, a Gaussian pulse is examined for the case of 2π pulse area. Results are exhibited in Figs. 5 and 6 and show that the sech pulse is better for the higher fidelity and the smaller population left in the excited state after the pulse.

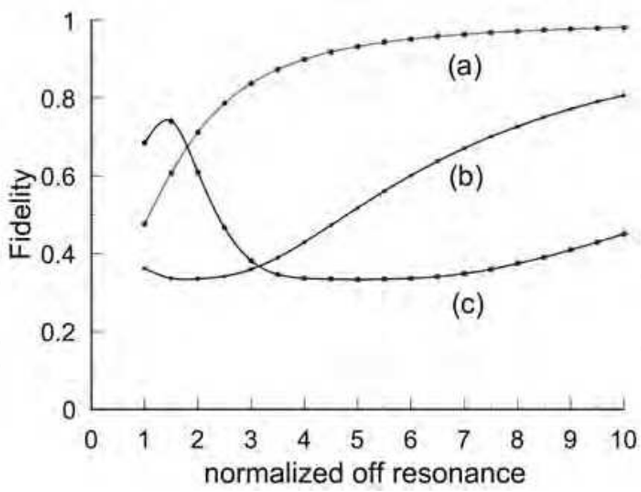

Fig. 3. Fidelity of the spin rotation of a single electron is plotted as a function of the normalized off-resonance. Curves (a), (b) and (c) correspond to the pulse area 2π, 4π and 6π, respectively.

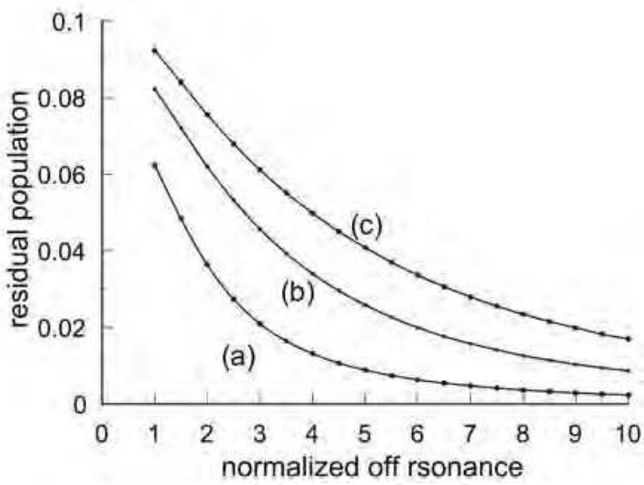

Fig. 4. Residual population in the excited state $|T\rangle$ after the spin rotation of a single electron is plotted as a function of the normalized off-resonance. Curves (a), (b) and (c) correspond to the pulse area 2π, 4π and 6π, respectively.

So far we have considered a typical Λ-type system composed of three energy levels. However, in the case of a singly charged semiconductor quantum dot, there are at least two excited states, namely the trion states, associated with two spin directions of the hole state. Thus, the four level system, as depicted in Fig. 7, is more appropriate. The fidelity of the spin rotation for the four level system is examined using the parameters:

$$\hbar\omega_T - \hbar\omega_{\bar{T}} = 0.05\text{meV}\ , \hbar\omega_{\bar{x}} - \hbar\omega_x = 0.05\text{meV}\ , \hbar\omega_x - \hbar\omega_y = 0.05\text{meV}\ , \tag{41}$$

$$\hbar\Gamma_{T\to x} = \hbar\Gamma_{T\to\bar{x}} = \hbar\Gamma_{\bar{T}\to x} = \hbar\Gamma_{\bar{T}\to\bar{x}} = 0.01\text{meV}\ , \tag{42}$$

$$\hbar\gamma_{T\,x} = \hbar\gamma_{T\,\bar{x}} = \hbar\gamma_{\bar{T}\,x} = \hbar\gamma_{\bar{T}\,\bar{x}} = 0.05\text{meV}\ , \tag{43}$$

where the Raman condition is applied to the left Λ-type transition. Results are given in Fig. 8 and show that the fidelity is not degraded by an additional Λ-type transition, especially for the 2π pulse area. Thus the spin rotation is expected to be robust against the overlap of several Λ-type transitions.

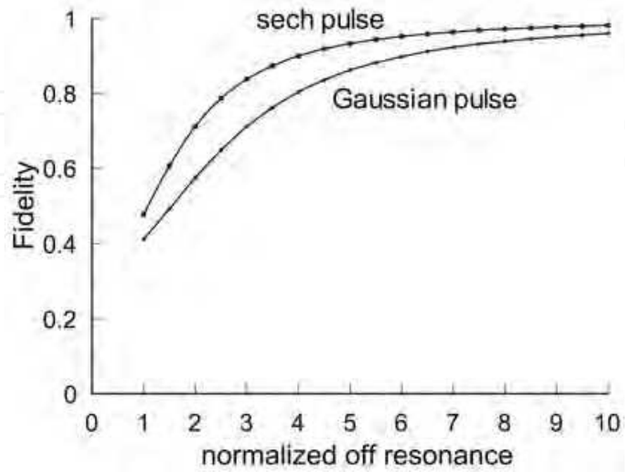

Fig. 5. Fidelity of the spin rotation of a single electron is compared between the cases of a Gaussian pulse and a sech pulse for the 2π pulse area.

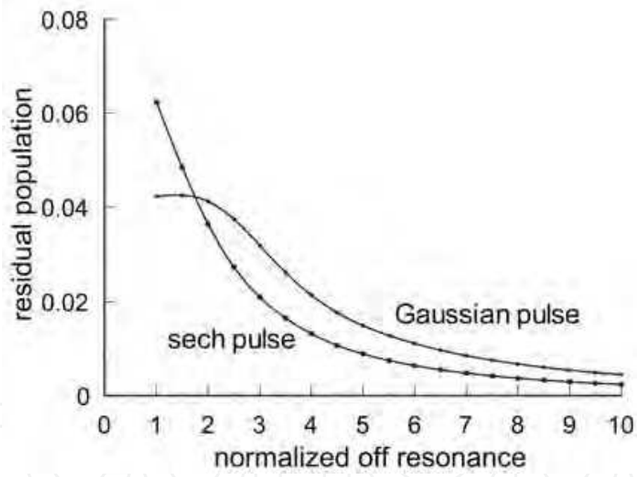

Fig. 6. Residual population in the excited state $|T\rangle$ after the spin rotation of a single electron is compared between the cases of a Gaussian pulse and a sech pulse for the 2π pulse area.

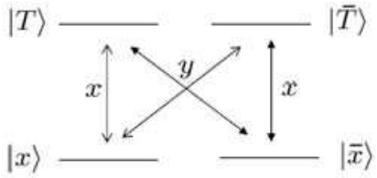

Fig. 7. Four level system composed of two electron spin states (lower levels) and two trion states with different hole spin states (upper levels). Allowed optical transitions are indicated by the x and y polarizations.

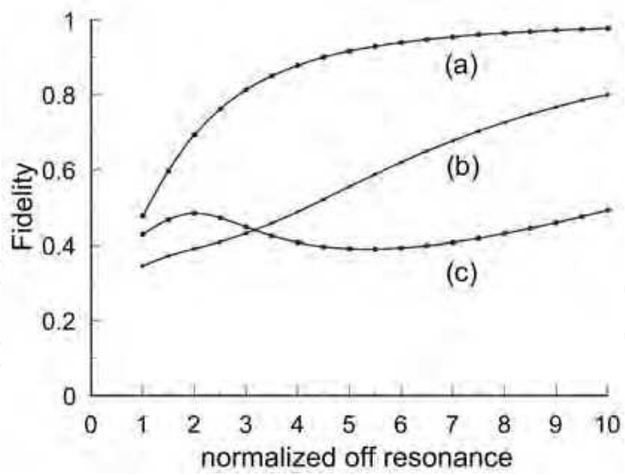

Fig. 8. Fidelity of the spin rotation of a single electron is plotted as a function of the normalized off-resonance in the four-level model. Curves (a), (b) and (c) correspond to the pulse area 2π, 4π and 6π, respectively.

3. Optical STIRAP method for spin rotation of two electrons

Now we extend the above arguments to the spin rotation of two electrons. This spin rotation is important because a qubit composed of the singlet state and one of the triplet states of two electrons confined in a semiconductor quantum dot was established and its electrical manipulation was demonstrated16. Here we examine the possibility of ultrafast spin otation of two electrons by an optical means. As discussed above, the essential ingredient is the Λ-type transition with mutually orthogonal optical selection rules which enables the spin rotation of an arbitrary angle along an arbitrary direction. In the Faraday configuration the allowed optical transitions are exhibited in Fig. 9. The charged exciton state is depicted by X^{2-}. An additional superscript indicates the spin direction of the electron in the excited orbital state and an additional subscript represents the spin direction of the heavy hole in the lowest energy orbital state, namely,

$$|hh+\rangle = |\frac{3}{2}\frac{3}{2}\rangle \ , \ |hh-\rangle = |\frac{3}{2} \ -\frac{3}{2}\rangle \ , \tag{44}$$

where the left hand side indicates the missing state of the valence band electron in the state on the right hand side. There is a Λ-type transition but with the same optical selection rules. Thus the arbitrary spin rotation is not possible.

On the other hand, for the Voigt configuration in which a magnetic field is applied along the quantum dot plane (taken as the x axis), the optical selection rules are exhibited in Fig. 10 for the case associated with the light hole state. Here, an additional superscript attached to X^{2-} indicates the spin direction of the electron in the excited orbital state, namely, +(-) for the $x(-x)$ direction and an additional subscript represents the spin direction of the light hole in the lowest energy orbital state, namely, $\ell h+$ or $\ell h-$ corresponding to

$$|lh+\rangle = \frac{1}{\sqrt{2}}(|\frac{3}{2}\frac{1}{2}\rangle + |\frac{3}{2} - \frac{1}{2}\rangle) \text{ or } |lh-\rangle = \frac{1}{\sqrt{2}}(-|\frac{3}{2}\frac{1}{2}\rangle + |\frac{3}{2} - \frac{1}{2}\rangle) \ , \tag{45}$$

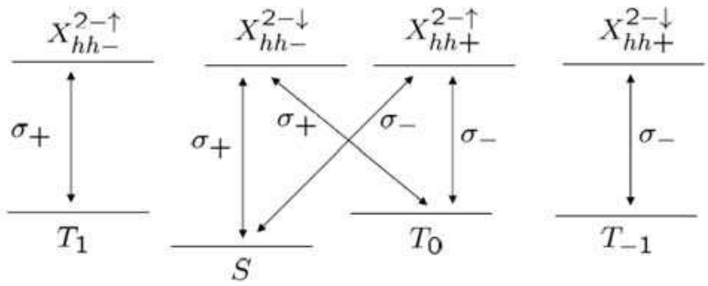

Fig. 9. Allowed optical transitions in the Faraday configuration for two electrons. The lower levels represent the four spin states of two electrons: the singlet (S) and three triplet (T_1, T_0, T_{-1}) states, whereas the upper levels exhibit the negatively doubly charged exciton states (X^{2-}) with indexes indicating the spin state of the electron in the excited orbital and the spin state of the heavy hole.

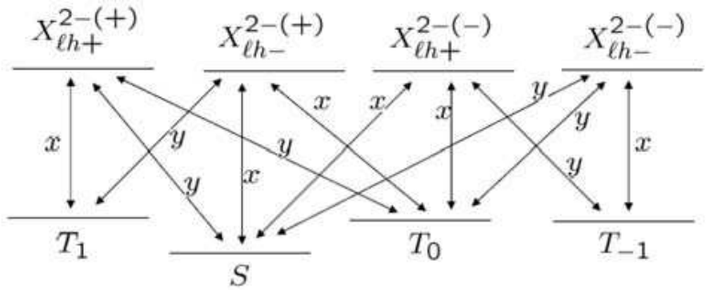

Fig. 10. Allowed optical transitions in the Voigt configuration for two electrons. The lower levels represent the four spin states of two electrons: the singlet (S) and three triplet (T_1, T_0, T_{-1}) states, whereas the upper levels exhibit the negatively doubly charged exciton states (X^{2-}) with indexes indicating the spin state of the electron in the excited orbital and the spin state of the light hole.

where the left hand side indicates the missing state of the valence band electron in the state on the right hand side. Then we find that the spin rotation by STIRAP is possible except for cases of the pseudospin composed of (S, T_0) and (T_1, T_{-1}). The same situation holds also for transitions associated with the heavy hole. As seen in Fig. 10, the four levels in both the ground and excited states are energetically close to each other. In the excited states, they are lying within the range determined by the Zeeman energy difference, which is about several tens of μeV for 1 Tesla. In the ground states, the singlet state lies below the triplet states by the orbital excitation energy and the triplet states are close to each other within the Zeeman energy difference.

It is important to examine the fidelity of the spin rotation under the situation that several Λ-type transitions are overlapping within a similar energy range. As a model system we consider a five-level system as depicted in Fig. 11. Relative energy differences, population relaxation and decoherence rates employed are

$$\hbar\omega_1 - \hbar\omega_3 = 0.05\text{meV}\ , \hbar\omega_2 - \hbar\omega_0 = 0.05\text{meV}\ , \hbar\omega_4 - \hbar\omega_0 = 0.07\text{meV}\ , \tag{46}$$

$$\hbar\Gamma_{1\to0} = \hbar\Gamma_{1\to2} = \hbar\Gamma_{1\to4} = \hbar\Gamma_{3\to0} = \hbar\Gamma_{3\to2} = \hbar\Gamma_{3\to4} = 0.01\text{meV}\ , \tag{47}$$

$$\hbar\gamma_{10} = \hbar\gamma_{12} = \hbar\gamma_{14} = \hbar\gamma_{30} = \hbar\gamma_{32} = \hbar\gamma_{34} = 0.05\text{meV}\ . \tag{48}$$

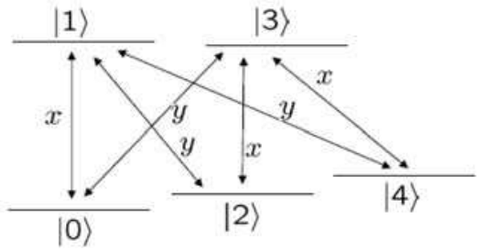

Fig. 11. Five level system composed of three lower levels and two upper levels. This is a simplest idealized model for studying the effect of overlapping Λ-type transitions.

Concerning the four levels composed of $|0\rangle$, $|1\rangle$, $|2\rangle$ and $|3\rangle$, the relevant parameters are the same as for the four-level system in Fig. 7. Thus, the effect of an additional level $|4\rangle$ can be examined. Results are exhibited in Fig. 12. An additional level degrades the coherence of the STIRAP process and reduces the fidelity of the spin rotation. However, in the case of 2π pulse area, the fidelity keeps a good value for large off-resonance energies.

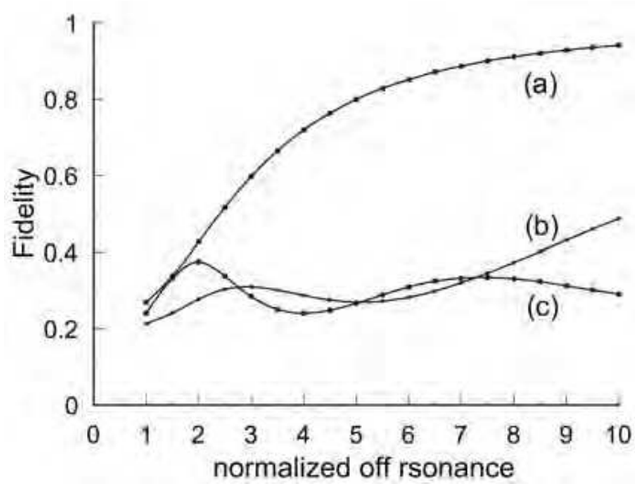

Fig. 12. Fidelity of the spin rotation of two electrons is plotted as a function of the normalized off-resonance in the five-level model. Curves (a), (b) and (c) correspond to the pulse area 2π, 4π and 6π, respectively.

Another important feature is the state initialization within the pseudospin subspace. When we want to rotate the pseudospin composed of $|0\rangle$ and $|2\rangle$ states in Fig. 11, the state should be initialized within this subspace. We examined the effect on the fidelity of the spin rotation of the incomplete state initialization. The fidelity is calculated for the case in which the state is prepared in the subspace spanned by the $|0\rangle$ and $|2\rangle$ states with the weight of 0.9 and in the $|4\rangle$ state with the weight of 0.1. Results are given in Fig. 13 with those for the complete initialization in which the state is prepared in the subspace spanned only by the $|0\rangle$ and $|2\rangle$ states. The fidelity loss proportional to the deviation from the perfect initialization is seen. Thus the state initialization should be carried out as perfect as possible. One possible way of the state initialization is the use of the singlet-triplet level crossing by the magnetic field tuning. At first we prepare the two electrons in the singlet state and then bring the system adiabatically to the crossing point. During the residence period at the crossing point,

the state mixing is induced by the spin-orbit interaction and the hyperfine interaction with nuclei, leading to an incoherent mixed state. This incoherent mixed state is sufficient to carry out the spin rotation. When the electron Zeeman energy is sufficiently large and three triplet states are well separated, the state initialization within the subspace composed of two crossing states such as (S, T_1), (S, T_0) and (S, T_{-1}) will be established.

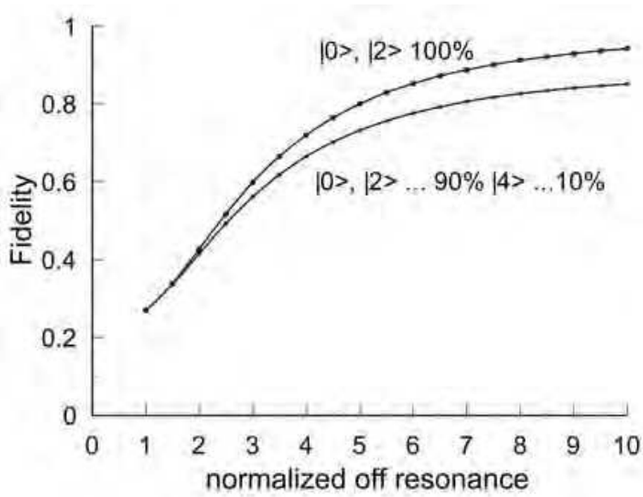

Fig. 13. Fidelity of the spin rotation of two electrons is plotted as a function of the normalized off-resonance in the five-level model for two cases, namely, one case where initially the population is prepared within the states $|0\rangle$ and $|2\rangle$ with 90% weight and in the state $|4\rangle$ with 10% weight and the other case where the population is prepared within the subspace spanned only by $|0\rangle$ and $|2\rangle$. The pulse area is 2π.

4. Spin state tomography of a single electron

The projective measurement of the spin state of a single electron is possible based on the Faraday/Kerr rotation of a linearly polarized light and this has been demonstrated experimentally very recently [42,43]. However, in the spin state tomography, all the components of the spin (s_x, s_y, s_z), namely, the off-diagonal (coherence) components as well as the diagonal components of the density matrix should be measured. The density matrix of a single electron spin in the spin up and down bases is given by

$$\rho = \begin{pmatrix} \rho^0_{\uparrow\uparrow} & \rho^0_{\uparrow\downarrow} \\ \rho^0_{\downarrow\uparrow} & \rho^0_{\downarrow\downarrow} \end{pmatrix} = \frac{1}{2}(1 + \vec{s}\cdot\vec{\sigma}) \quad \text{with} \quad \vec{s} = (s_x, s_y, s_z)\ , \tag{49}$$

$$s_x = \mathrm{Tr}\ \rho\sigma_x = \rho^0_{\downarrow\uparrow} + \rho^0_{\uparrow\downarrow}\ ,\ s_y = \mathrm{Tr}\ \rho\sigma_y = -i(\rho^0_{\downarrow\uparrow} - \rho^0_{\uparrow\downarrow})\ ,\ s_z = \mathrm{Tr}\ \rho\sigma_z = \rho^0_{\uparrow\uparrow} - \rho^0_{\downarrow\downarrow}\ , \tag{50}$$

where σ_i (i = x, y, z) is the Pauli spin matrix. The purity of this state is given by

$$\mathcal{P} = \mathrm{Tr}\rho^2 = \frac{1}{2}(1 + (\vec{s})^2)\ . \tag{51}$$

Thus, by measuring all the components (s_x, s_y, s_z) we can determine whether the state is a pure state or not.

In order to measure all the components (s_x, s_y, s_z) by an optical means, there should be at least one excited state which is connected to both the spin up and spin down states of the electron, in other words, there should be a Λ -type transition. This transition creates the coherence between the spin up and spin down states, rotates the spin and enables the spin state tomography. It is easily shown that such a Λ -type transition is not possible in the Faraday configuration. On the other hand, in the Voigt configuration in which an in-plane magnetic field is applied along, e.g., the x direction, the Λ-type transition is possible as depicted in Fig. 14 for the optical transitions associated with both the heavy hole and light hole states. In Fig.14, the optical polarization selection rules are given in the x and y bases. The excited state is a trion state composed of a spin-singlet electron pair and a hole. The electron and hole states under an in-plane magnetic field are described by

$$|x+\rangle = \frac{1}{\sqrt{2}}(|\uparrow\rangle + |\downarrow\rangle)\ ,\ |x-\rangle = \frac{1}{\sqrt{2}}(-|\uparrow\rangle + |\downarrow\rangle)\ , \tag{52}$$

$$|hh+\rangle = \frac{1}{\sqrt{2}}(|\frac{3}{2}\frac{3}{2}\rangle + |\frac{3}{2}-\frac{3}{2}\rangle)\ ,\ |hh-\rangle = \frac{1}{\sqrt{2}}(-|\frac{3}{2}\frac{3}{2}\rangle + |\frac{3}{2}-\frac{3}{2}\rangle)\ , \tag{53}$$

$$|lh+\rangle = \frac{1}{\sqrt{2}}(|\frac{3}{2}\frac{1}{2}\rangle + |\frac{3}{2}-\frac{1}{2}\rangle)\ ,\ |lh-\rangle = \frac{1}{\sqrt{2}}(-|\frac{3}{2}\frac{1}{2}\rangle + |\frac{3}{2}-\frac{1}{2}\rangle)\ , \tag{54}$$

where for the hole states the left hand side represents the missing state of the valence band electron in the state on the right hand side.

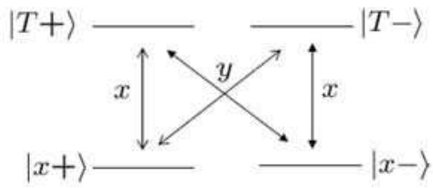

Fig. 14. Λ-type transitions for a single electron in the Voigt configuration. The lower levels indicate the two spin states of the electron, whereas the upper levels represent the trion states associated with the light hole or the heavy hole states. The polarization selection rules are given in terms of the x and y bases, where the in-plane magnetic field is applied in the x direction.

Now we discuss the scheme to measure the spin component of the electron. A probe light propagates along the z axis and its polarization rotation is measured in the transmission or reflection geometry. Thus the dielectric tensor represented in the bases of the electric field components in the x and y directions is relevant. In the theoretical analysis a single Λ-type transition will be considered with the level indexes as depicted in Fig. 15. An external test field is applied to estimate the dielectric tensor and is assumed as

$$\vec{\mathcal{E}}_{\rm test}(t) = (\mathcal{E}_x\ \vec{e}_x + \mathcal{E}_y\ \vec{e}_y)e^{i\omega t} + \text{c.c.}\ , \tag{55}$$

where $\vec{e}_x(\vec{e}_y)$ is the unit vector in the $x(y)$ direction. The initial density matrix, which is to be fixed from the measurements, is given by

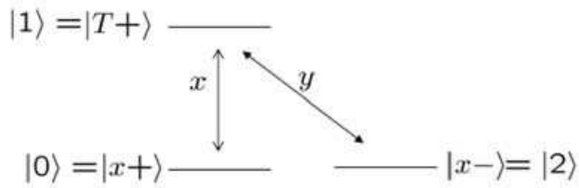

Fig. 15. A Λ-type transition is chosen from the left hand side of Fig. 14 and the levels are numbered to simplify theoretical expressions.

$$\rho(t=0) = \begin{pmatrix} \rho_{00}^0 & \rho_{02}^0 & 0 \\ \rho_{20}^0 & \rho_{22}^0 & 0 \\ 0 & 0 & 0 \end{pmatrix} , \tag{56}$$

where the bases are chosen as $|0\rangle$, $|2\rangle$ and $|1\rangle$. The relevant equations of motion for the density matrix take the form:

$$\dot{\rho} = -\frac{i}{\hbar}[H_0 + V, \rho] + \Gamma\rho , \tag{57}$$

where H_0 and V are similar to those in Eqs. (2) and (3) and Γ includes the population relaxation and decoherence terms. Expressions for each matrix element are given below:

$$\dot{\rho}_{00} = i\Omega_x e^{i\omega t}\rho_{10} - i\Omega_x^* e^{-i\omega t}\rho_{01} + \Gamma_{1\to 0}\rho_{11} , \tag{58}$$

$$\dot{\rho}_{11} = -i\Omega_x e^{i\omega t}\rho_{10} - i\Omega_y e^{i\omega t}\rho_{12} + \text{c.c.} - (\Gamma_{1\to 0} + \Gamma_{1\to 2})\rho_{11} , \tag{59}$$

$$\rho_{22} = 1 - \rho_{00} - \rho_{11} , \tag{60}$$

$$\dot{\rho}_{01} = i\Omega_x e^{i\omega t}(\rho_{11} - \rho_{00}) - i\Omega_y e^{i\omega t}\rho_{02} + (i\omega_{10} - \gamma_{01})\rho_{01} , \tag{61}$$

$$\dot{\rho}_{02} = i\Omega_x e^{i\omega t}\rho_{12} - i\Omega_y^* e^{-i\omega t}\rho_{01} + (i\omega_{20} - \gamma_{02})\rho_{02} , \tag{62}$$

$$\dot{\rho}_{12} = i\Omega_x^* e^{-i\omega t}\rho_{02} + i\Omega_y^* e^{-i\omega t}(\rho_{22} - \rho_{11}) + (i\omega_{21} - \gamma_{12})\rho_{12} \tag{63}$$

$$\text{with} \qquad \Omega_x = \frac{\mu_{01}^x \mathcal{E}_x}{\hbar} , \ \Omega_y = \frac{\mu_{21}^y \mathcal{E}_y}{\hbar} , \ \omega_{ij} = (E_i - E_j)/\hbar , \tag{64}$$

where μ_{ij}^k is the optical matrix element between the states $|i\rangle$ and $|j\rangle$ for the light polarization in the k direction, E_i the energy of the state $|i\rangle$, $\Gamma_{i\to j}$ the population decay rate from the state $|i\rangle$ to the state $|j\rangle$ and γ_{ij} is the decay rate of the coherence between the states $|i\rangle$ and $|j\rangle$. In order to facilitate the analysis, the rapidly oscillating parts will be separated out as

$$\rho_{01}(t) = \bar{\rho}_{01}(t)e^{i\omega t} , \ \rho_{12}(t) = \bar{\rho}_{12}(t)e^{-i\omega t} , \tag{65}$$

where $\bar{\rho}_{01}$ and $\bar{\rho}_{12}$ are slowly varying amplitudes. ρ_{02} is also slowly varying because ω_{02} is very small compared with the optical transition energies. Then the equations of motion for these amplitudes become

$$\dot{\bar{\rho}}_{01} = i\Omega_x(\rho_{11} - \rho_{00}) - i\Omega_y\rho_{02} + (i(\omega_{10} - \omega) - \gamma_{01})\bar{\rho}_{01} \ , \tag{66}$$

$$\dot{\rho}_{02} = i\Omega_x\bar{\rho}_{12} - i\Omega_y^*\bar{\rho}_{01} + (i\omega_{20} - \gamma_{02})\rho_{02} \ , \tag{67}$$

$$\dot{\bar{\rho}}_{12} = i\Omega_x^*\rho_{02} + i\Omega_y^*(\rho_{22} - \rho_{11}) + (i(\omega - \omega_{12}) - \gamma_{12})\bar{\rho}_{12} \ . \tag{68}$$

The stationary solutions within the linear response to the test field are given by

$$\rho_{01}^{st} = \frac{i\Omega_x\rho_{00}^0 + i\Omega_y\rho_{02}^0}{i\Delta - \gamma_{01}} \ , \ \rho_{21}^{st} = \frac{i\Omega_x\rho_{20}^0 + i\Omega_y\rho_{22}^0}{i(\Delta - \omega_{20}) - \gamma_{21}} \quad \text{with} \ \ \Delta = \omega_{10} - \omega \ . \tag{69}$$

Now the induced polarization and the corresponding susceptibility tensor χ are derived as

$$\vec{P} = \mathrm{Tr}\ \vec{\mu}\rho^{st} = (\mu_{10}^x\rho_{01}^{st} + \mu_{12}^y\rho_{21}^{st})e^{i\omega t} + \text{c.c.} \tag{70}$$

$$= \overleftrightarrow{\chi} \cdot \vec{\mathcal{E}}\ e^{i\omega t} + \text{c.c.} = \begin{pmatrix} \chi_{xx} & \chi_{xy} \\ \chi_{yx} & \chi_{yy} \end{pmatrix} \begin{pmatrix} \mathcal{E}_x \\ \mathcal{E}_y \end{pmatrix} e^{i\omega t} + \text{c.c.} \tag{71}$$

Assuming the large off-resonance: $\Delta \gg \omega_{20}$, γ_{ij} , we have

$$\overleftrightarrow{\chi}_A = A \begin{pmatrix} \rho_{00}^0 & i\rho_{02}^0 \\ -i\rho_{20}^0 & \rho_{22}^0 \end{pmatrix} \ \text{with} \ \ A = \frac{|\mu_{01}^x|^2}{v_0\hbar\Delta} \ , \tag{72}$$

where v_0 is the normalization volume for the polarization density and the subscript A is attached for the later use. The dielectric tensor is given by

$$\overleftrightarrow{\varepsilon} = \varepsilon_0 + 4\pi\ \overleftrightarrow{\chi}_A \ , \tag{73}$$

where ε_0 is the background dielectric constant. In the case of large off-resonance, another Λ-type transition depicted in Fig. 16 should also be taken into account. After a similar calculation, the corresponding susceptibility $\overleftrightarrow{\chi}_B$ is estimated as

$$\overleftrightarrow{\chi}_B = B \begin{pmatrix} \rho_{22}^0 & i\rho_{20}^0 \\ -i\rho_{02}^0 & \rho_{00}^0 \end{pmatrix} \ \text{with} \ \ B = \frac{|\mu_{2\tilde{1}}^x|^2}{v_0\hbar\tilde{\Delta}} \ \text{and} \ \tilde{\Delta} = \omega_{\tilde{1}2} - \omega \ . \tag{74}$$

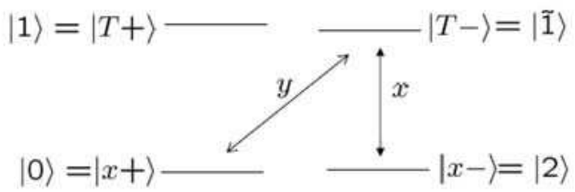

Fig. 16. A Λ-type transition is chosen from the right hand side of Fig. 14 and the levels are numbered to simplify theoretical expressions.

When the trion state associated with the heavy hole is considered, $\Delta \cong \tilde{\Delta}$ and hence $A \cong B$, because the g-factor of the heavy hole is very small. In the absence of the coupling between the heavy hole (hh) and the light hole (lh), the in-plane g-factor of the heavy hole is zero.

Actually, that g-factor is finite due to the hh-lh coupling. However, the g-factor of the heavy hole is one order of magnitude smaller than that of the light hole [25,44]. Then the total susceptibility becomes

$$\overleftrightarrow{\chi}_{\text{tot.}}=\overleftrightarrow{\chi}_A+\overleftrightarrow{\chi}_B\cong A\begin{pmatrix}1 & i(\rho^0_{20}+\rho^0_{02})\\ -i(\rho^0_{20}+\rho^0_{02}) & 1\end{pmatrix}. \tag{75}$$

This indicates that only one component of the spin vector can be monitored. On the other hand, in the case of the light hole, the energy difference between $|1\rangle$ and $|\tilde{1}\rangle$ is rather large and the contribution from either $\overleftrightarrow{\chi}_A$ or $\overleftrightarrow{\chi}_B$ is dominant. Then all the spin components can be measured as discussed below.

Now we discuss the measurement schemes to probe the spin components. For the moment, we consider the transmission geometry, assuming that the $\overleftrightarrow{\chi}_A$ is dominantly contributing to the dielectric tensor. Then the susceptibility tensor can be written in terms of s_x, s_y and s_z in Eq. (50) as

$$\overleftrightarrow{\chi}_A=\frac{A}{2}\begin{pmatrix}1+s_z & is_x+s_y\\ -is_x+s_y & 1-s_z\end{pmatrix} \tag{76}$$

and the dielectric tensor is written as

$$\overleftrightarrow{\varepsilon}=\varepsilon_0+4\pi\,\overleftrightarrow{\chi}_A=(\varepsilon_0+2\pi A)\,\overleftrightarrow{1}+4\pi\,\overleftrightarrow{\chi}'_A \tag{77}$$

$$\text{with}\qquad \overleftrightarrow{\chi}'_A=\frac{A}{2}\begin{pmatrix}s_z & is_x+s_y\\ -is_x+s_y & -s_z\end{pmatrix}=\frac{A}{2}\left[{}^t\vec{s}\cdot\vec{n}\;{}^t\vec{n}\cdot\vec{\sigma}+(\vec{\sigma}\times\vec{s})\cdot\vec{n}\right], \tag{78}$$

where $\vec{n}\;{}^t\vec{n}$ is a dyadic form and the last expression is general for the axially symmetric case with the propagation vector $\vec{n}$ of the probe light. Here $\overleftrightarrow{\chi}'_A$ is a Hermitian matrix and has eigenvectors associated with real eigenvalues χ_1 and χ_2, namely

$$\overleftrightarrow{\chi}'_A\;\vec{u}_1=\chi_1\,\vec{u}_1\,,\;\overleftrightarrow{\chi}'_A\;\vec{u}_2=\chi_2\,\vec{u}_2\,. \tag{79}$$

Then a probe light with an amplitude:

$$\vec{\mathcal{E}}_{\text{probe}}(t,z=0)=(a\,\vec{u}_1+b\,\vec{u}_2)\,e^{i\omega t}+\text{c.c.}=\vec{\mathcal{E}}^{(+)}_{\text{probe}}\,e^{i\omega t}+\text{c.c.} \tag{80}$$

propagates as

$$\vec{\mathcal{E}}_{\text{probe}}(t,z)=[a\,\vec{u}_1e^{-ik_0\sqrt{\varepsilon_1}z}+b\,\vec{u}_2\,e^{-ik_0\sqrt{\varepsilon_2}z}]\,e^{i\omega t}+\text{c.c.} \tag{81}$$

$$\text{with}\quad k_0=\frac{\omega}{c}\;\text{and}\;\;\varepsilon_{1(2)}=\varepsilon_0+2\pi A+4\pi\chi_{1(2)}=\tilde{\varepsilon}_0+4\pi\chi_{1(2)}\,. \tag{82}$$

For a thin sample, e.g., a single quantum dot layer, $k_0z\ll1$ and the phase factor can be expanded with respect to this smallness parameter. Then the transmitted field is obtained as

$$\vec{\mathcal{E}}_{\rm probe}(t,z) = e^{i\omega t - ik_0\sqrt{\tilde{\varepsilon}_0}z}[a\ \vec{u}_1 + b\ \vec{u}_2 - i\frac{2\pi k_0 z}{\sqrt{\tilde{\varepsilon}_0}}(a\ \chi_1\vec{u}_1 + b\ \chi_2\vec{u}_2) + \cdots] + \text{c.c.} \tag{83}$$

$$= e^{i\omega t - ik_0\sqrt{\tilde{\varepsilon}_0}z}[\overleftrightarrow{1} - i\eta\ \overleftrightarrow{\chi}'_A + \cdots]\vec{\mathcal{E}}^{(+)}_{\rm probe} + \text{c.c. with } \eta = \frac{2\pi k_0 z}{\sqrt{\tilde{\varepsilon}_0}}\,. \tag{84}$$

Now we can discuss the schemes to measure the spin components. Here the polarization of the probe light is specified in a definite direction and the transmitted probe light is passed through a polarizing beam splitter (PBS). Then the intensity difference between two orthogonally polarized components is measured. In the first measurement, the probe light is polarized along the x direction and the transmitted light is given by

$$\vec{\mathcal{E}}_{\rm trans.} = [\overleftrightarrow{1} - i\eta\ \overleftrightarrow{\chi}'_A]\ \vec{\mathcal{E}}_{\rm probe} = [\overleftrightarrow{1} - i\eta\ \overleftrightarrow{\chi}'_A]\ \begin{pmatrix}1\\0\end{pmatrix} = \begin{pmatrix}1 - i\eta A s_z/2\\ -\eta A(s_x + is_y)/2\end{pmatrix}\,. \tag{85}$$

When this transmitted light is analyzed in the diagonal(D) and cross-diagonal($\bar{D}$) polarization bases, namely,

$$|D\rangle = \frac{1}{\sqrt{2}}\begin{pmatrix}1\\1\end{pmatrix}\ ,\ |\bar{D}\rangle = \frac{1}{\sqrt{2}}\begin{pmatrix}1\\-1\end{pmatrix}\ , \tag{86}$$

the intensity difference is calculated as

$$|\langle D|\vec{\mathcal{E}}_{\rm trans.}\rangle|^2 - |\langle \bar{D}|\vec{\mathcal{E}}_{\rm trans.}\rangle|^2 \cong -\eta A\ s_x + \mathcal{O}((\eta A)^2)\,. \tag{87}$$

Thus the s_x component can be measured. In the second measurement, the probe light is polarized along the x direction and the transmitted light is analyzed in the right-circular(R) and left-circular(L) polarization bases, namely,

$$|R\rangle = \frac{1}{\sqrt{2}}\begin{pmatrix}1\\i\end{pmatrix}\ ,\ |L\rangle = \frac{1}{\sqrt{2}}\begin{pmatrix}1\\-i\end{pmatrix}\,. \tag{88}$$

Then the intensity difference is given by

$$|\langle R|\vec{\mathcal{E}}_{\rm trans.}\rangle|^2 - |\langle L|\vec{\mathcal{E}}_{\rm trans.}\rangle|^2 \cong -\eta A\ s_y + \mathcal{O}((\eta A)^2) \tag{89}$$

and the s_y component can be measured. In the third measurement, the probe light is polarized along the diagonal(D) direction and the transmitted light is given by

$$\vec{\mathcal{E}}_{\rm trans.} = [\overleftrightarrow{1} - i\eta\ \overleftrightarrow{\chi}'_A]\ \vec{\mathcal{E}}_{\rm probe} \text{ with } \quad \vec{\mathcal{E}}_{\rm probe} = \frac{1}{\sqrt{2}}\begin{pmatrix}1\\1\end{pmatrix} \tag{90}$$

$$= \frac{1}{\sqrt{2}}\begin{pmatrix}1 + \eta A s_x/2 - i\eta A(s_y + s_z)/2\\ 1 - \eta A s_x/2 - i\eta A(s_y - s_z)/2\end{pmatrix}\,. \tag{91}$$

This transmitted light is analyzed in the right-circular(R) and left-circular(L) polarization bases. Then the intensity difference is calculated as

$$|\langle R|\vec{\mathcal{E}}_{\rm trans.}\rangle|^2 - |\langle L|\vec{\mathcal{E}}_{\rm trans.}\rangle|^2 \cong \eta A\, s_z + \mathcal{O}((\eta A)^2) \tag{92}$$

and the s_z component can be measured. Thus, all the spin components (s_x, s_y, s_z) are measured and the spin state tomography is completed.

These measurement schemes can be extended to the reflection geometry. Assuming the normal incidence of the probe light, the amplitude of the reflected light is calculated as

$$\vec{\mathcal{E}}_{\rm ref.} = \frac{1-\sqrt{\tilde{\varepsilon}}}{1+\sqrt{\tilde{\varepsilon}}}\,\vec{\mathcal{E}}_{\rm probe} = \frac{1-\sqrt{\tilde{\varepsilon}_0}(\overleftrightarrow{1} + \frac{2\pi\overleftrightarrow{\chi}'_A}{\tilde{\varepsilon}_0} + \cdots)}{1+\sqrt{\tilde{\varepsilon}_0}(\overleftrightarrow{1} + \frac{2\pi\overleftrightarrow{\chi}'_A}{\tilde{\varepsilon}_0} + \cdots)}\,\vec{\mathcal{E}}_{\rm probe} \tag{93}$$

$$= \frac{1-\sqrt{\tilde{\varepsilon}_0}}{1+\sqrt{\tilde{\varepsilon}_0}}\,[\overleftrightarrow{1} + \frac{4\pi\,\overleftrightarrow{\chi}'_A}{(\tilde{\varepsilon}_0-1)\sqrt{\tilde{\varepsilon}_0}} + \cdots]\,\vec{\mathcal{E}}_{\rm probe} \tag{94}$$

$$= \frac{1-\sqrt{\tilde{\varepsilon}_0}}{1+\sqrt{\tilde{\varepsilon}_0}}\,[\overleftrightarrow{1} + \eta\,\overleftrightarrow{\chi}'_A + \cdots]\,\vec{\mathcal{E}}_{\rm probe} \quad \text{with} \quad \eta = \frac{4\pi}{(\tilde{\varepsilon}_0-1)\sqrt{\tilde{\varepsilon}_0}}\,. \tag{95}$$

Here the first factor is arising from the background dielectric constant and is not relevant in discussing the dependence of the reflected light amplitude on the polarization configuration. The reflected light amplitude denoted by $\vec{\mathcal{E}}_{\rm Kerr}$ is introduced by

$$\vec{\mathcal{E}}_{\rm Kerr} = [\overleftrightarrow{1} + \eta\,\overleftrightarrow{\chi}'_A + \cdots]\,\vec{\mathcal{E}}_{\rm probe}\,. \tag{96}$$

Then the measurement of the spin components can be achieved as follows. In the first scheme, the polarization of the probe light is chosen along the x direction and the reflected light is given by

$$\vec{\mathcal{E}}_{\rm Kerr} = [\overleftrightarrow{1} + \eta\,\overleftrightarrow{\chi}'_A + \cdots]\,\vec{\mathcal{E}}_{\rm probe} \quad \text{with} \quad \vec{\mathcal{E}}_{\rm probe} = \begin{pmatrix} 1 \\ 0 \end{pmatrix} \tag{97}$$

$$= \begin{pmatrix} 1+\eta A s_z/2 \\ \eta A(-is_x + s_y)/2 \end{pmatrix}\,. \tag{98}$$

This reflected light is analyzed in terms of the right-circular (R) and left-circular (L) polarization bases. Then the intensity difference is given by

$$|\langle R|\vec{\mathcal{E}}_{\rm Kerr}\rangle|^2 - |\langle L|\vec{\mathcal{E}}_{\rm Kerr}\rangle|^2 \cong -\eta A\, s_x + \mathcal{O}((\eta A)^2)\,. \tag{99}$$

Thus the s_x component can be measured. In the second scheme, the polarization of the probe light is chosen along the x direction and the reflected light is analyzed in terms of the diagonal (D) and cross-diagonal ($\bar{D}$) polarization bases. Then the intensity difference is given by

$$|\langle D|\vec{\mathcal{E}}_{\rm Kerr}\rangle|^2 - |\langle \bar{D}|\vec{\mathcal{E}}_{\rm Kerr}\rangle|^2 \cong \eta A\, s_y + \mathcal{O}((\eta A)^2) \tag{100}$$

and the s_y component can be measured. In the third scheme, the polarization of the probe light is chosen along the diagonal (D) direction, namely

$$\vec{\mathcal{E}}_{\rm probe} = |D\rangle = \frac{1}{\sqrt{2}} \begin{pmatrix} 1 \\ 1 \end{pmatrix} \tag{101}$$

and the reflected light is analyzed in terms of the horizontal (x) and vertical (y) polarization bases. Then the intensity difference is given by

$$|\langle H|\vec{\mathcal{E}}_{\rm Kerr}\rangle|^2 - |\langle V|\vec{\mathcal{E}}_{\rm Kerr}\rangle|^2 \cong \eta A \, s_z + \mathcal{O}((\eta A)^2) \tag{102}$$

and the s_z component can be measured. In this way, all the spin components (s_x, s_y, s_z) can be measured and the spin state tomography of a single electron is completed.

5. Quantum correlation (Bell) measurement between two electrons

In the scheme of quantum repeater, the primary elements are the quantum state transfer between a photon and an electron and the entanglement swapping through the Bell (correlation) measurement between two electrons which are created through the quantum state transfer from two photons. It is preferable to do the Bell measurement between electrons instead of photons because the mismatch between the photon arrival times can be compensated by the rather long coherence time of electrons, whereas the storage of photons is rather difficult although the techniques for the photon storage are progressing steadily. Thus we start the discussion assuming that two electrons are prepared in a semiconductor nanostructure, e.g., a quantum dot. We propose an optical method to measure the spin state of two electrons based on the Faraday or Kerr rotation. Here we employ a linearly polarized off-resonant probe light and measure the orientation of the transmitted (reflected) light. Thus the method can be nondestructive in the same sense as demonstrated for the case of a single electron [42,43].

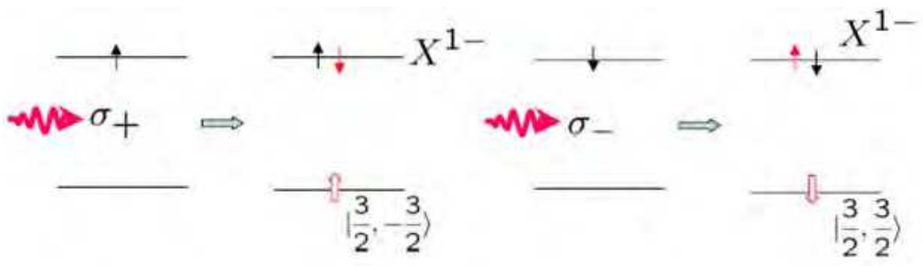

Fig. 17. Elementary processes of the Faraday rotation for the case of a single resident electron. $\sigma_{+(-)}$ denotes the right (left) circularly polarized light. The upper (lower) horizontal line indicates the electron (hole) level. A thin (thick empty) arrow represents an electron (a hole) with the spin direction along the arrow.

Before going into details, let us review briefly the elementary processes of the Faraday rotation for the case of a single electron. We consider a III-V semiconductor quantum dot in which the hole ground state is the heavy hole state and a magnetic field is applied along the crystal growth direction (namely, perpendicular to the quantum well plane). As is well

known, the right-circularly polarized light denoted by σ_+ excites a down spin electron from the valence band state $|3/2, -3/2\rangle$ creating a charged exciton or trion, while the left-circularly polarized light denoted by σ_-excites an up spin electron from the valence band state $|3/2, 3/2\rangle$, as exhibited in Fig. 17. When we probe the system with a linearly polarized light along the x direction, i.e.,

$$|x\rangle = \frac{1}{\sqrt{2}}(|\sigma_+\rangle + |\sigma_-\rangle) \,, \tag{103}$$

where $\sigma_+(\sigma_-)$ may be alternatively denoted by $R(L)$ for the right (left) circular polarization, one of the circular components receives a phase shift and the Faraday rotation occurs. Thus we can distinguish the two spin states of an electron by the sign of the Faraday rotation angle.

Now we extend this argument to the case of two electrons and consider relevant elementary processes for four states of two electrons, namely, the singlet state(S) and the triplet states with the magnetic quantum number 1, 0 and -1 (T_1, T_0, T_{-1}). For the T_1 state, spins of the two resident electrons are aligned in the same direction and a σ_+ polarized light excites a down spin electron from the valence band creating a doubly negatively charged exciton X^{2-}, as shown in Fig. 18, in which the lowest electron orbital state is occupied by a spin-singlet electron pair and the spin direction of the electron in the second lowest orbital state is indicated in the superscript and the spin direction of the heavy hole is depicted in the subscript, namely:

$$|\Uparrow\rangle = |\frac{3}{2}\ -\frac{3}{2}\rangle \,, \ |\Downarrow\rangle = |\frac{3}{2}\ \frac{3}{2}\rangle \,, \tag{104}$$

where the left hand side represents the missing state of the valence band electron in the state on the right hand side. The T_1 state is optically inactive for the σ_- polarized light. For the T_{-1} state, a σ_- polarized light excites an up spin electron from the valence band creating another doubly negatively charged exciton. This T_{-1} state is optically inactive for the σ_+ polarized light. Thus these two states can be distinguished by the sign of the Faraday rotation angle. On the other hand, the S and T_0 states are optically active for both circular polarizations as exhibited in Figs. 19 and 20, and the sign of the Faraday rotation angle is determined by the competition between the phase shifts for each circular component.

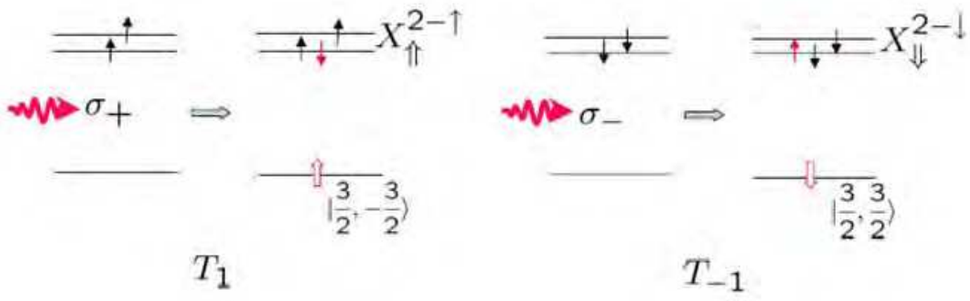

Fig. 18. Elementary processes of the Faraday rotation for the triplet T_1 and T_{-1} states of two resident electrons.

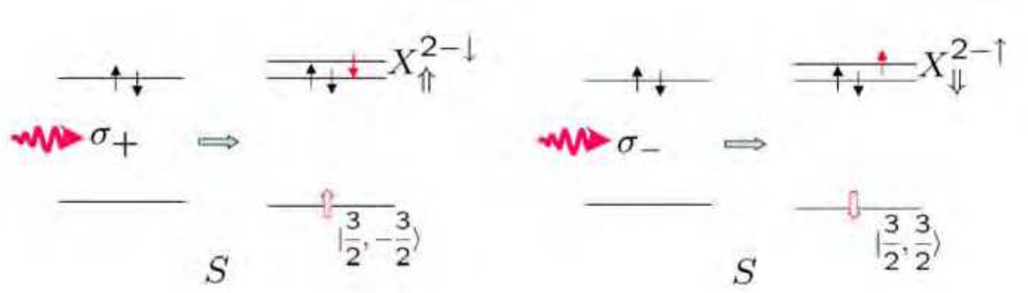

Fig. 19. Elementary processes of the Faraday rotation for the singlet S state of two resident electrons.

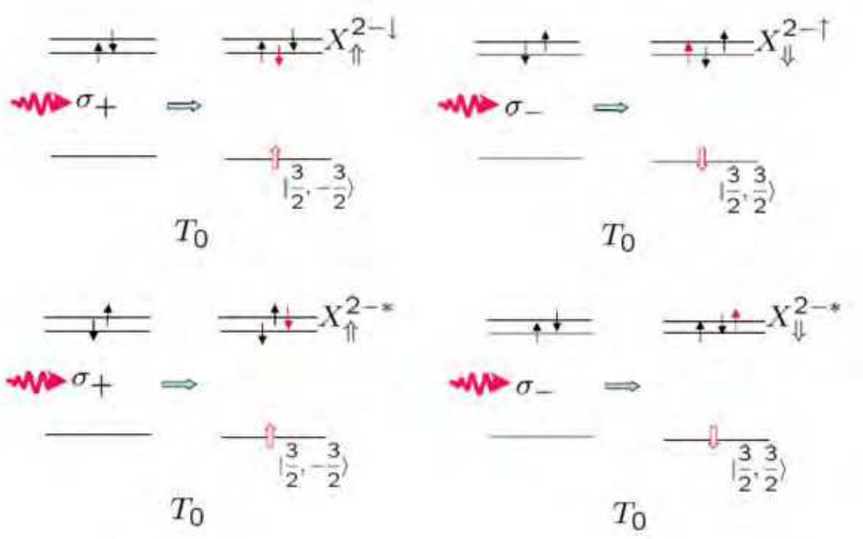

Fig. 20. Elementary processes of the Faraday rotation for the triplet T_0 state of two resident electrons. $X_{\Uparrow}^{2-*}$ and $X_{\Downarrow}^{2-*}$ denote excited states of the doubly negatively charged exciton.

The expression of the Faraday rotation angle is obtained in the perturbation theory and is composed of two terms:

$$\varphi \propto \sum_{j(\sigma+)} \frac{|\langle j|P_{\sigma+}|i\rangle|^2(E_{j,i}-\hbar\omega)}{(\hbar^2\gamma_{j,i}^2+(E_{j,i}-\hbar\omega)^2)} - \sum_{k(\sigma-)} \frac{|\langle k|P_{\sigma-}|i\rangle|^2(E_{k,i}-\hbar\omega)}{(\hbar^2\gamma_{k,i}^2+(E_{k,i}-\hbar\omega)^2)}, \tag{105}$$

where i indicates the initial state of two electrons, j (k) the final state of the optical transition for the σ_+ (σ_-) component, $E_{a,b} = E_a - E_b$ with E_a being the energy of the a state, $\gamma_{a,b}$ the dephasing rate corresponding to the $a \leftrightarrow b$ transition and $\hbar\omega$ denotes the photon energy of the linearly polarized probe light. As mentioned before, for the T_1 state only the σ_+ transitions contribute, whereas for the T_{-1} state only the σ_- transitions contribute. Thus the two states can be distinguished by the sign of the Faraday rotation angle. For the S and T_0 states, both σ_+ and σ_- transitions contribute and thus more detailed arguments are necessary to determine the sign of the Faraday rotation angle. Now we examine the resonance position of the Faraday rotation angle with respect to the probe photon energy $\hbar\omega$. From the

elementary processes exhibited in Figs. 18-20, it is seen that for the triplet states the resonance occurs at around the energy of the doubly charged exciton states ($E(X^{2-})$). On the other hand, for the singlet state the resonance occurs at a higher energy than $E(X^{2-})$ because the lowest orbital state is already occupied by a spin-singlet electron pair and the optical transition should occur to the higher orbital state.

Now we discuss more details of the Faraday rotation angle for the case of T_0 state. As mentioned before, both σ_+ and σ_- circular components contribute to the Faraday rotation. The lowest-energy final state of the optical transition for each circular component is given by

$$j(\sigma+) = X_{\Uparrow}^{2-\downarrow} , \qquad k(\sigma-) = X_{\Downarrow}^{2-\uparrow} . \tag{106}$$

The energies of these states are different in a magnetic field because the spin configuration is different for these states. In terms of the electron g-factor $g_{c(v)}$ for the conduction (valence) band, these energies are given as

$$E(X_{\Uparrow}^{2-\downarrow}) \cong -\frac{1}{2}(g_c\mu_B B - g_v\mu_B B) + E_0 , \tag{107}$$

$$E(X_{\Downarrow}^{2-\uparrow}) \cong \frac{1}{2}(g_c\mu_B B - g_v\mu_B B) + E_0 , \tag{108}$$

where E_0 is the lowest energy of the interband transition. Then the energy difference $|E(X_{\Uparrow}^{2-\downarrow}) - E(X_{\Downarrow}^{2-\uparrow})|$ is typically about one tenth of meV for a magnetic field about 1 Tesla and is comparable to the dephasing rate of the optical transitions. From the formula in Eq. (105) we see that the dependence of the Faraday rotation angle on the probe photon energy is determined by the difference between two dispersive curves with nearly equal resonance energies. Thus the profile is given by the derivative of the dispersive curve as shown in Fig. 21, depending on the sign of the energy difference. The same situation holds for the singlet state S.

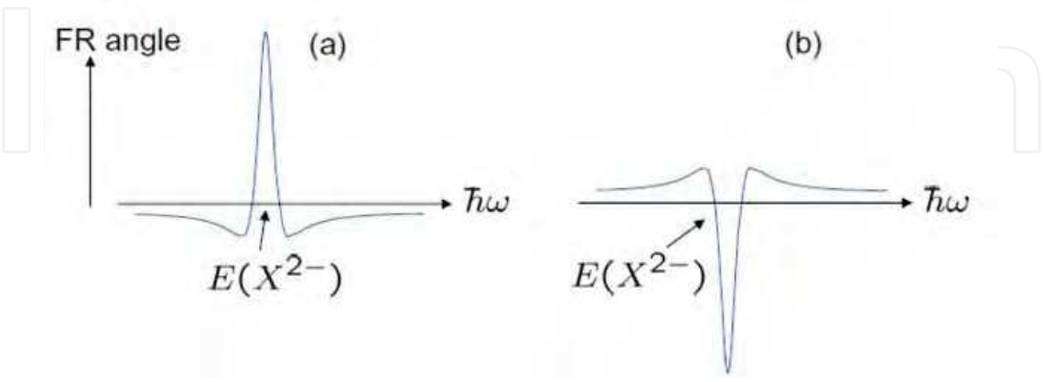

Fig. 21. Dependence on the probe photon energy ($\hbar\omega$) of the Faraday rotation angle for the triplet T_0 state and the singlet S state of two resident electrons. It depends on the sign of the energy difference; namely, (a) $|E(X_{\Uparrow}^{2-\downarrow}) - E(X_{\Downarrow}^{2-\uparrow})| > 0$, (b) $|E(X_{\Uparrow}^{2-\downarrow}) - E(X_{\Downarrow}^{2-\uparrow})| < 0$

Summarizing these considerations, we can show the schematic dependence of the Faraday rotation angle on the probe photon energy in Fig. 22. The triplet states T_1 and T_{-1} exhibit a typical dispersive lineshape. On the other hand, the profile for the triplet T_0 and the singlet S states is given by the derivative of the dispersive curve, where the case of $|E(X_{\Uparrow}^{2-\downarrow}) - E(X_{\Downarrow}^{2-\uparrow})| > 0$ is assumed. The resonance occurs at around the energy of the doubly charged exciton state denoted by $E(X^{2-})$ for the triplet states, whereas for the singlet state it occurs at a higher energy than $E(X^{2-})$ by the orbital excitation energy Δ_e. Thus when we choose the probe photon energy at the downward arrow as shown in Fig. 22, the Faraday rotation angle is positive for the T_1 state and is negative for the T_{-1} state. For the T_0 state, the Faraday rotation angle is negative but the magnitude is small. For the singlet S state, the Faraday rotation angle would be vanishingly small because of the large off-resonance. Consequently, we can distinguish between the four states of two electrons by the magnitude and the sign of the Faraday rotation angle.

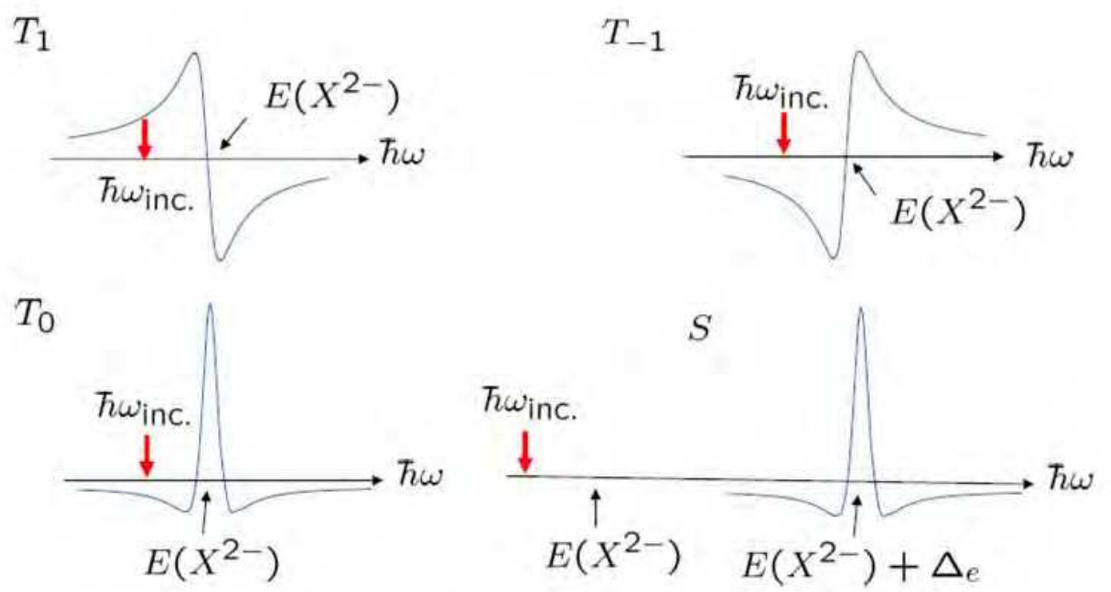

Fig. 22. Dependence on the probe photon energy ($\hbar\omega$) of the Faraday rotation angle for the three triplet states T_1, T_0, T_{-1} and the singlet state S of two resident electrons. Those for T_0 and S are exhibited for the case of $|E(X_{\Uparrow}^{2-\downarrow}) - E(X_{\Downarrow}^{2-\uparrow})| > 0$.

Now we discuss relevant parameters to optimize the Faraday rotation measurement. The essential requirement is the preparation of the lowest two orbital states which are energetically well-separated from higher excited states. We consider a circularly symmetric GaAs quantum dot with parabolic lateral confinement under a magnetic field along the growth direction. Then the orbital eigenstates are represented by the Fock-Darwin states [45,46] whose eigenenergies are given by

$$E_{\nu,n} = (|n| + 1 + 2\nu)\hbar\Omega + \frac{n}{2}\hbar\omega_c \ \text{ with } \ \Omega = \sqrt{\omega_0^2 + \frac{\omega_c^2}{4}}\ , \ \omega_c = \frac{eB}{m^*c}\ , \tag{109}$$

where ω_0 is the frequency of the harmonic confinement in the lateral direction and m^* is the electron effective mass. When we employ the parameter values: $\hbar\omega_0$ = 5meV, B = 5T and m^* = $0.067m_0$ with m_0 being the free electron mass, we have $\hbar\omega_c$ = 8.7meV and $\hbar\Omega$ = 6.63meV. The lowest two orbital levels have the spacing of 2.3 meV and are well-separated from the higher orbital level by 8.7 meV. These parameter values would enable the Faraday rotation measurement to be carried out reliably.

6. Spin state tomography of two electrons

In the last Section, we discussed the projective measurement of the spin state of two electrons in a semiconductor quantum dot based on the Faraday or Kerr rotation. The method can project an arbitrary spin state onto one of the singlet and three triplet states by a single-shot measurement. However, in order to know the spin state precisely, namely, the density matrix in the spin space, we have to achieve the spin state tomography. This tomography cannot be carried out by a single-shot measurement but repeated measurements are necessary under the assumption that exactly the same spin state can be prepared repeatedly. This tomography will be necessary to estimate, for example, the degree of the entanglement between two electrons created at distant locations after photo-absorption of a pair of polarization entangled photons. The tomographic methods for a single photon and two photons were already established [47] and it is instructive to review the tomography of the photon states in considering the spin state tomography.

Photons have two orthogonal polarization states, namely, horizontal (H) and vertical (V) polarizations denoted by

$$|H\rangle = \begin{pmatrix} 1 \\ 0 \end{pmatrix} , \; |V\rangle = \begin{pmatrix} 0 \\ 1 \end{pmatrix} . \tag{110}$$

The photon density matrix, which is a 2×2 matrix, can be decomposed as

$$\rho = \frac{1}{2}(\overleftrightarrow{1} + \vec{s} \cdot \vec{\sigma}) \quad \text{with} \quad s_i = \mathrm{Tr}\, \rho\sigma_i \quad (i = x,\ y,\ z) , \tag{111}$$

where s_i's are the Stokes parameters and σ_i's are the Pauli spin operators. These parameters can be fixed by the apparatus exhibited typically in Fig. 23. The polarizer is assumed to transmit only the vertically polarized photons. The fast axes of the quarter wave plate (QWP) and the half wave plate (HWP) are adjusted to select a particular polarization component. In the $|H\rangle$ and $|V\rangle$ bases, an arbitrary photon state is given by

$$\begin{pmatrix} \bar{a} \\ \bar{b} \end{pmatrix} = a\,|H\rangle + b\,|V\rangle , \tag{112}$$

where a and b are arbitrary complex constants satisfying the normalization condition: $|a\rangle^2$ + $|b\rangle^2$ = 1. Then the role of the HWP is described by

$$\begin{pmatrix} \bar{a} \\ \bar{b} \end{pmatrix} = U_{HWP}(h) \begin{pmatrix} a \\ b \end{pmatrix} \quad \text{with} \quad U_{HWP}(h) = \begin{pmatrix} \cos 2h & -\sin 2h \\ -\sin 2h & -\cos 2h \end{pmatrix} , \tag{113}$$

where the left hand side is the photon state after transmission through the HWP and h denotes the angle between the fast axis of the HWP and the vertical direction. In the same way, the effect of the QWP is described by

$$\begin{pmatrix} \bar{a} \\ \bar{b} \end{pmatrix} = U_{QWP}(q) \begin{pmatrix} a \\ b \end{pmatrix} \quad \text{with} \quad U_{QWP}(q) = -e^{i\pi/4} \frac{1}{\sqrt{2}} \begin{pmatrix} i - \cos 2q & \sin 2q \\ \sin 2q & i + \cos 2q \end{pmatrix} , \quad (114)$$

where q denotes the angle between the fast axis of the QWP and the vertical direction. Thus the polarization state of photons which can be transmitted to the detector is given by

$$\begin{pmatrix} a \\ b \end{pmatrix} = U^{\dagger}_{QWP}(q) U^{\dagger}_{HWP}(h) \begin{pmatrix} 0 \\ 1 \end{pmatrix} = \frac{1}{\sqrt{2}} \begin{pmatrix} i \sin 2h + \sin 2(h-q) \\ i \cos 2h - \cos 2(h-q) \end{pmatrix} . \quad (115)$$

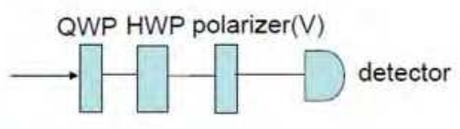

Fig. 23. Apparatus to select a particular polarization component of light. It is composed of a half wave plate (HWP), a quarter wave plate (QWP), a polarizer which is assumed to transmit only a vertically polarized photon, and a photon detector.

polarization	h	q
$\|H\rangle$	$\pi/4$	0
$\|V\rangle$	0	0
$\|D\rangle$	$\pi/8$	$\pi/4$
$\|R\rangle$	$\pi/8$	0

Table I. Combinations of the angles h and q of the fast axes of the HWP and QWP to select a particular polarization component of light

The four bases of measurement are exhibited as

$$|H\rangle = \begin{pmatrix} 1 \\ 0 \end{pmatrix} , \; |V\rangle = \begin{pmatrix} 0 \\ 1 \end{pmatrix} , |D\rangle = \frac{1}{\sqrt{2}} \begin{pmatrix} 1 \\ 1 \end{pmatrix} , |R\rangle = \frac{1}{\sqrt{2}} \begin{pmatrix} 1 \\ i \end{pmatrix} , \quad (116)$$

where $D(R)$ denotes the diagonally (right-circularly) polarized photon. These photon states can be selected by choosing the angles of the fast axes of the HWP and QWP as given in Table I. Then the photon count rates for these polarizations are calculated as

$$N_H \propto \mathrm{Tr}\rho|H\rangle\langle H| = \frac{1}{2}(1 + s_z) , \; N_V \propto \mathrm{Tr}\rho|V\rangle\langle V| = \frac{1}{2}(1 - s_z) , \quad (117)$$

$$N_D \propto \mathrm{Tr}\rho|D\rangle\langle D| = \frac{1}{2}(1 + s_x) , \; N_R \propto \mathrm{Tr}\rho|R\rangle\langle R| = \frac{1}{2}(1 - s_y) \quad (118)$$

and the Stokes parameters can be estimated by

$$s_x = 2\frac{N_D}{N_0} - 1 , \; s_y = 1 - 2\frac{N_R}{N_0} , \; s_z = \frac{N_H - N_V}{N_0} \quad \text{with} \quad N_0 = N_H + N_V . \quad (119)$$

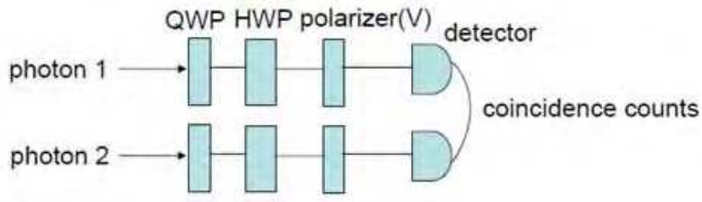

Fig. 24. Parallel combination of two apparatus to select a particular polarization component of photons.

The extension of this scheme to the state tomography of two photons is straightforward [47]. We prepare parallel lines of apparatus as depicted in Fig. 24. By measuring the coincidence counts for sixteen combinations of the angles of the fast axes of two HWPs and two QWPs, we can fix the sixteen parameters $\{r_{ij}\}(I, j = 0, 1, 2, 3)$ which specify the density matrix for two photons:

$$\rho = \sum_{i,j=0}^{3} r_{ij}\, \sigma_i^1 \otimes \sigma_j^2 \ , \tag{120}$$

where the superscript 1(2) indicates the first (second) photon.
Now we proceed to the spin state tomography of electrons. Extension of the above arguments to the electron spin state tomography is straightforward using the correspondence:

$$|H\rangle \leftrightarrow |\uparrow\rangle \ , \ |V\rangle \leftrightarrow |\downarrow\rangle \ , \tag{121}$$

where $|\uparrow\rangle(|\downarrow\rangle)$ indicates the spin up (down) state of the electron. But the devices corresponding to the HWP and QWP should be prepared for the electron. This can be realized by making use of the difference in the spin precession angle due to the Zeeman energy splitting. In a magnetic field along the z axis, the spin state evolves in time as

$$\begin{pmatrix} a \\ b \end{pmatrix} \rightarrow \begin{pmatrix} e^{-i\omega_z t} a \\ e^{i\omega_z t} b \end{pmatrix} = e^{-i\omega_z t} \begin{pmatrix} a \\ e^{i2\omega_z t} b \end{pmatrix} \ , \tag{122}$$

where $\hbar\omega_z$ is the Zeeman energy for the up-spin electron. The spin HWP (QWP) can be achieved by employing a square-shaped pulsed magnetic field and by adjusting the pulse duration and the field amplitude as $2\omega_z t = \pi(\pi/2)$. The angle of the fast axis corresponds to the tilt angle of the magnetic field. For example, when the tilt angle of the magnetic field is h relative to the z axis, the spin eigenstates are given by

$$|\uparrow\rangle_h = \begin{pmatrix} \cos\frac{h}{2} \\ \sin\frac{h}{2} \end{pmatrix} \ , \ |\downarrow\rangle_h = \begin{pmatrix} -\sin\frac{h}{2} \\ \cos\frac{h}{2} \end{pmatrix} \ . \tag{123}$$

Then the effect of the "spin" HWP is represented by

$$\begin{pmatrix} \bar{a} \\ \bar{b} \end{pmatrix} = U^s_{HWP}(h) \begin{pmatrix} a \\ b \end{pmatrix} \quad \text{with} \quad U^s_{HWP}(h) = \begin{pmatrix} \cos h & \sin h \\ \sin h & -\cos h \end{pmatrix} \ . \tag{124}$$

In a similar way, the effect of the "spin" QWP is given as

$$\begin{pmatrix} \bar{a} \\ \bar{b} \end{pmatrix} = U^s_{QWP}(q) \begin{pmatrix} a \\ b \end{pmatrix} \quad \text{with} \quad U^s_{QWP}(q) = e^{i\pi/4} \frac{1}{\sqrt{2}} \begin{pmatrix} -i + \cos q & \sin q \\ \sin q & -i - \cos q \end{pmatrix} , \quad (125)$$

where q is the tilt angle of the magnetic field in the "spin" QWP.

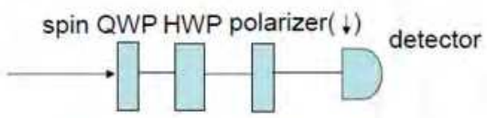

Fig. 25. Apparatus to select a particular spin component of an electron. It is composed of a spin half wave plate (spin HWP), a spin quarter wave plate (spin QWP), a spin polarizer which is assumed to transmit only the down spin electron, and an electron detector.

Now that the basic elements are prepared, we can consider the apparatus for the spin state tomography, as depicted in Fig. 25, which is basically the same as that for the photon case except for the replacement of the HWP and QWP by the spin HWP and spin QWP, respectively. The spin polarizer is assumed to transmit only the down spin electron based on the difference in the Faraday rotation angle. This polarizer should have the ability to measure the single electron spin. Consequently, the apparatus depicted in Fig. 25 filters out the state given by

$$\begin{pmatrix} a \\ b \end{pmatrix} = U^{s\,\dagger}_{QWP}(q) U^{s\,\dagger}_{HWP}(h) \begin{pmatrix} 0 \\ 1 \end{pmatrix} = \frac{1}{\sqrt{2}} \begin{pmatrix} i \sin h + \sin(h-q) \\ -i \cos h + \cos(h-q) \end{pmatrix} . \quad (126)$$

spin direction	h	q
$\lvert\uparrow_z\rangle$	$\pi/2$	0
$\lvert\downarrow_z\rangle$	0	0
$\lvert\downarrow_x\rangle$	$\pi/4$	$\pi/2$
$\lvert\downarrow_y\rangle$	$\pi/4$	0

Table II. Combinations of the angles h and q of the fast axes of the spin HWP and spin QWP to select a particular spin component of an electron.

Thus by choosing the angles h and q as exhibited in Table II, the apparatus can filter out those spin states in the Table. The spin state tomography can be carried out in the same manner as that for the photon. The extension of the spin state tomography to the case of two electrons is straightforward. We prepare a parallel set of the apparatus for a single electron as depicted in Fig. 26. Coincidence counts of electrons for sixteen combinations of the angles of the fast axes of two spin HWPs and two spin QWPs can determine, in completely the same way as in the case of two photons, the sixteen parameters $\{r_{ij}\}$ (i, j = 0, 1, 2, 3) of the density matrix of the electron spins:

$$\rho = \sum_{i,j=0}^{3} r_{ij}\, \sigma_i^1 \otimes \sigma_j^2 , \quad (127)$$

where the superscript 1(2) indicates the first (second) electron.

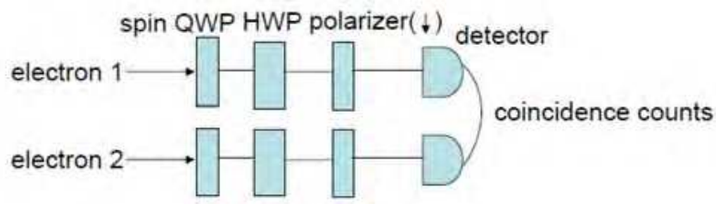

Fig. 26. Parallel combination of two apparatus to select a particular spin component of electrons.

7. Summary

We have investigated theoretically the STIRAP method based on the Λ-type optical transitions for the unitary spin rotation of both a single electron and two electrons and discussed the optimal conditions to minimize the residual population left in the intermediate excited states after the process. The 2π pulse with a large off-resonance energy would be better but the rotation angle is small. Thus, for the rotation of a large angle, multiple pulses would be necessary. For the two-electrons spin qubit, several Λ-type transitions are closely overlapping in the narrow energy range and the Raman condition should be tuned precisely to single out a particular Λ-type transition. It is absolutely necessary to confirm the quantum state of the electron after the spin manipulation, namely, to examine whether the electron spin is prepared in the desired state or not. This requires the full state tomography. We have proposed the methods of the spin state tomography based on the Faraday or Kerr rotation for both cases of a single electron and two electrons. Another fundamental process in the quantum information processing is the Bell (quantum correlation) measurement for the entanglement swapping. This is a single-shot projective measurement in contrast to the full state tomography. We proposed an optical method to distinguish between the four states of two electrons based on the Faraday or Kerr rotation and confirmed the feasibility.

As a prospect in the near future, we can construct hopefully a secure and robust system of the quantum repeater combining the established results, namely, the efficient quantum state transfer between a photon and an electron spin [37, 38, 48], the reliable Bell measurement of two electrons for the entanglement swapping based on the Faraday or Kerr rotation and the longlived quantum memory based on nuclear spins [49, 50].

8. Acknowledgments

We would like to thank Professor H. Kosaka for stimulating discussions and continual encouragements. We appreciate very much the financial supports from the CREST project of the Japan Science and Technology Agency, from the SCOPE program of the Ministry of Internal Affairs and Communications, and from the Ministry of Education, Culture, Sports, Science and Technology, Japan. The numerical calculation in this work has been done using the facilities of the Supercomputer Center, Institute for Solid State Physics, University of Tokyo.

9. References

[1] A. Barenco, D. Deutsch, A. Ekert, and R. Jozsa, "Conditional quantum dynamics and logic gates," *Phys. Rev. Lett.* 74, 4083–4086 (1995).

[2] D. Loss and D. P. DiVincenzo, "Quantum computation with quantum dots," *Phys. Rev. A* 57, 120-126 (1998).

[3] A. Imamoglu, D. D. Awschalom, G. Burkard, D. P. DiVincenzo, D. Loss, M. Sherwin, and A. Small, "Quantum information processing using quantum dot spins and cavity QED," *Phys. Rev. Lett.* 83, 4204-4207 (1999).

[4] C. H. Bennett and D. P. DiVincenzo, "Quantum information and computation," *Nature* 404, 247–255 (2000).

[5] M. A. Nielsen and I. L. Chuang (Eds.), *Quantum Computation and Quantum Information*, Cambridge University Press, Cambridge (2000).

[6] D. Bouwmeester, A. Ekert and A. Zeilinger (Eds.), *The Physics of Quantum Information*, Springer- Verlag, Berlin (2000).

[7] D. D. Awschalom, D. Loss and N. Samarth (Eds.), *Semiconductor Spintronics and Quantum Computation*, Springer-Verlag, Berlin (2002).

[8] T. Takagahara (Ed.), *Quantum Coherence, Correlation and Decoherence in Semiconductor Nanostructures*, Academic Press, Elsevier, New York (2003).

[9] T. Takagahara (Ed.), *Proceedings of the International Symposium on Photonics and Spintronics in Semiconductor Nanostructures* (PSSN 2003, Kyoto) available online at http://www.

[10] X. Li, Y. Wu, D. G. Steel, D. Gammon, T. H. Stievater, D. S. Katzer, D. Park, C. Piermarocchi, and L. J. Sham, "An all-optical quantum gate in a semiconductor quantum dot," *Science* 301, 809-811 (2003).

[11] R. Hanson, L. P. Kouwenhoven, J. R. Petta, S. Tarucha, and L. M. Vandersypen, "Spins in fewelectron quantum dots", *Rev. Mod. Phys.* 79, 1217 (2007).

[12] Dyakonov, M. I. (Ed.), *Spin Physics in Semiconductors*, Springer-Verlag, Berlin (2008).

[13] Henneberger, F. and Benson, O. (Eds.), *Semiconductor Quantum Bits*, Pan Stanford Publishing Pte. Ltd., Singapore (2009).

[14] R. Hanson, B. Witkamp, L. M. K. Vandersypen, L. H. Willems van Beveren, J. M. Elzerman, and L. P. Kouwenhoven, "Zeeman energy and spin relaxation in a one-electron quantum dot," *Phys. Rev. Lett.* 91, 196802 (2003).

[15] M. Kroutvar, Y. Ducommun, D. Heiss, M. Bichler, D. Schuh, G. Abstreiter, and J. J. Finley, "Optically programmable electron spin memory using semiconductor quantum dots," *Nature* 432, 81-84 (2004).

[16] J. R. Petta, A. C. Johnson, J. M. Taylor, E. A. Laird, A. Yacoby, M. D. Lukin, C. M. Marcus, M. P. Hanson, and A. C. Gossard, "Coherent manipulation of coupled electron spins in semiconductor quantum dots," *Science* 309, 2180-2184 (2005).

[17] F. H. L. Koppens, C. Buizert, K. J. Tielrooij, I. T. Vink, K. C. Nowack, T. Meunier, L. P. Kouwenhoven, and L. M. K. Vandersypen, "Driven coherent oscillations of a single electron spin in a quantum dot," *Nature* 442, 766-771 (2006).

[18] T. Meunier, I. T. Vink, L. H. Willems van Beveren, K. J. Tielrooij, R. Hanson, F. H. L. Koppens, H. P. Tranitz, M. Wegscheider, L. P. Kouwenhoven, and L. M. K. Vandersypen, "Experimental signature of phonon-mediated spin relaxation in a two-electron quantum dot," *Phys. Rev. Lett.* 98, 126601 (2007).

[19] H. Kosaka, A. A. Kiselev, F. A. Baron, K. W. Kim, and E. Yablonovitch, "Electron g factor engineering in III-V semiconductors for quantum communications," *Electron. Lett.* 37, 464-465 (2001).

[20] R. Vrijen and E. Yablonovitch, "A spin-coherent semiconductor photo-detector for quantum communication," *Physica E* 10, 569-575 (2001).

[21] E. Yablonovitch, H. W. Jiang, H. Kosaka, H. D. Robinson, D. S. Rao, and T. Szkopek, "Optoelectronic quantum telecommunications based on spins in semiconductors," *Proc. IEEE* 91, 761-780 (2003).

[22] H. Kosaka and E. Yablonovitch, "Quantum media converter from a photon qubit to an electronspin qubit for quantum repeaters," in *Proceedings of the International Symposium on Photonics and Spintronics in Semiconductor Nanostructures* (PSSN 2003, Kyoto), T. Takagahara, Ed., pp. 63-70 (2003).

[23] M. Atatüre, J. Dreiser, A. Badolato, A. Hogele, K. Karrai, and A. Imamoglu, "Quantum-dot spin-state preparation with near-unity fidelity," *Science* 312, 551-553 (2006).

[24] C. Emary, X. Xu, D. G. Steel, S. Saikin, and L. J. Sham, "Fast Initialization of the Spin State of an Electron in a Quantum Dot in the Voigt Configuration", *Phys. Rev. Lett.* 98, 047401 (2007).

[25] X. Xu, Y. Wu, Bo Sun, Q. Huang, J. Cheng, D. G. Steel, A. S. Bracker, D. Gammon, C. Emary, and L. J. Sham, "Fast Spin State Initialization in a Singly Charged InAs-GaAs Quantum Dot by Optical Cooling", *Phys. Rev. Lett.* 99, 097401 (2007).

[26] K. C. Nowack, F. H. L. Koppens, Yu. V. Nazarov, and L. M. K. Vandersypen, "Coherent Control of a Single Electron Spin with Electric Fields", *Science* 318, 1430-1433 (2007).

[27] P. Chen, C. Piermarocchi, L. J. Sham, D. Gammon, and D. G. Steel , "Theory of quantum optical control of a single spin in a quantum dot", *Phys. Rev. B* 69, 075320 (2004).

[28] M. V. G. Dutt, J. Cheng, B. Li, X. Xu, Xiaoqin Li, P. R. Berman, D. G. Steel, A. S. Bracker, D. Gammon, S. E. Economou, R. B. Liu, and L. J. Sham, "Stimulated and spontaneous optical generation of electron spin coherence in charged GaAs quantum dots," *Phys. Rev. Lett.* 94, 227403 (2005).

[29] S. E. Economou and L. J. Sham, Y. Wu and D. G. Steel, "Proposal for optical U(1) rotations of electron spin trapped in a quantum dot", *Phys. Rev. B* 74, 205415 (2006).

[30] Y. Wu, E. D. Kim, X. Xu, J. Cheng, D. G. Steel, A. S. Bracker, D. Gammon, S. E. Economou, and L. J. Sham, "Selective Optical Control of Electron Spin Coherence in Singly Charged GaAs-Al0.3Ga0.7As Quantum Dots", *Phys. Rev. Lett.* 99, 097402 (2007).

[31] S. E. Economou and T. L. Reinecke, "Theory of Fast Optical Spin Rotation in a Quantum Dot Based on Geometric Phases and Trapped States", *Phys. Rev. Lett.* 99, 217401 (2007).

[32] J. Berezovsky, M. H. Mikkelsen, N. G. Stoltz, L. A. Coldren, and D. D. Awschalom, "Picosecond Coherent Optical Manipulation of a Single Electron Spin in a Quantum Dot", *Science* 320 349-352 (2008).

[33] D. Press, T. D. Ladd, B. Zhang, Y. Yamamoto, "Complete quantum control of a single quantum dot spin using ultrafast optical pulses", *Nature* 456, 218-221 (2008).

[34] A. M. Tyryshkin, S. A. Lyon, A. V. Astashkin, and A. M. Raitsimring, "Electron spin relaxation times of phosphorus donors in silicon", *Phys. Rev. B* 68, 193207 (2003).

[35] M. V. Gurudev Dutt, L. Childress, L. Jiang, E. Togan, J. Maze, F. Jelezko, A. S. Zibrov, P. R. Hemmer, and M. D. Lukin, "Quantum Register Based on Individual Electronic and Nuclear Spin Qubits in Diamond", *Science* 316, 1312-1316 (2007).

[36] J. J. L. Morton, A. M. Tyryshkin, R. M. Brown, S. Shankar, B. W. Lovett, A. Ardavan, T. Schenkel, E. E. Haller, J. W. Ager, S. A. Lyon, "Solid-state quantum memory using the 31P nuclear spin", *Nature* 455, 1085-1088 (2008).

[37] H. Kosaka, H. Shigyou, Y. Mitsumori, Y. Rikitake, H. Imamura, T. Kutsuwa, K. Arai, and K. Edamatsu, "Coherent Transfer of Light Polarization to Electron Spins in a semiconductor", *Phys. Rev. Lett.* 100, 096602 (2008).

[38] H. Kosaka, T. Inagaki, Y. Rikitake, H. Imamura, Y. Mitsumori, K. Edamatsu, "Spin state tomography of optically injected electrons in a semiconductor", *Nature* 457, 702-705 (2009).

[39] N. Rosen and C. Zener, "Double Stern-Gerlach Experiment and Related Collision Phenomena", *Phys. Rev.* 40, 502 - 507 (1932).

[40] A. Bambini and P. R. Berman, "Analytic solutions to the two-state problem for a class of coupling potentials", *Phys. Rev. A* 23, 2496 - 2501 (1981).

[41] M. Abramowitz and I. A. Stegun (Ed.), *Handbook of Mathematical Functions*, Dover Publications, Inc., New York (1972).

[42] J. Berezovsky, M. H. Mikkelsen, O. Gywat, N. G. Stoltz, L. A. Coldren, and D. D. Awschalom, "Nondestructive optical measurements of a single electron spin in a quantum dot," *Science* 314, 1916-1920 (2006).

[43] M. Atature, J. Dreiser, A. Badolato, and A. Imamoglu, "Observation of Faraday rotation from a single confined spin," *Nature Phys.* 3, 101-106 (2007).

[44] A. A. Kiselev, K. W. Kim and E. Yablonovitch, "In-plane light-hole g factor in strained cubic heterostructures", *Phys. Rev. B* 64, 125303 (2001).

[45] R. B. Dingle, "Some magnetic properties of metals. I. general introduction, and properties of large systems of electrons," *Proc. R. Soc. London, Ser. A* 211, 500-516 (1952).

[46] R. B. Dingle, "Some magnetic properties of metals. III. diamagnetic resonance," *Proc. R. Soc. London, Ser. A* 212, 38-47 (1952).

[47] D. F. V. James, P. G. Kwiat, W. J. Munro, and A. G. White, "Measurement of qubits", *Phys. Rev. A* 64, 052312 (2001).

[48] T. Takagahara and O. Cakir, "Theoretical aspects of quantum state transfer, correlation measurement and electron-nuclei coupled dynamics in quantum dots", *J. Nanophotonics* 1, 011593 (2007).

[49] J. M. Taylor, C. M. Marcus, and M. D. Lukin, "Long-lived memory for mesoscopic quantum bits," *Phys. Rev. Lett.* 90, 206803 (2003).

[50] O. Cakir and T. Takagahara, "Quantum dynamics in electron-nuclei coupled spin system in quantum dots: Bunching, revival, and quantum correlation in electron-spin measurements", *Phys. Rev. B* 77, 115304 (2008).

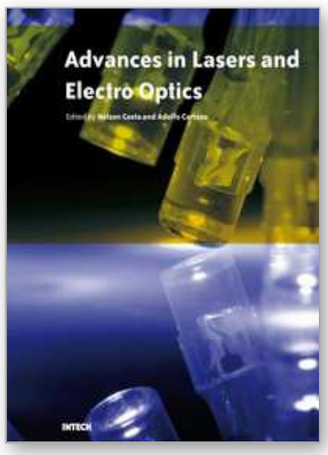

Advances in Lasers and Electro Optics

Edited by Nelson Costa and Adolfo Cartaxo

ISBN 978-953-307-088-9
Hard cover, 838 pages
Publisher InTech
Published online 01, April, 2010
Published in print edition April, 2010

Lasers and electro-optics is a field of research leading to constant breakthroughs. Indeed, tremendous advances have occurred in optical components and systems since the invention of laser in the late 50s, with applications in almost every imaginable field of science including control, astronomy, medicine, communications, measurements, etc. If we focus on lasers, for example, we find applications in quite different areas. We find lasers, for instance, in industry, emitting power level of several tens of kilowatts for welding and cutting; in medical applications, emitting power levels from few milliwatt to tens of Watt for various types of surgeries; and in optical fibre telecommunication systems, emitting power levels of the order of one milliwatt. This book is divided in four sections. The book presents several physical effects and properties of materials used in lasers and electro-optics in the first chapter and, in the three remaining chapters, applications of lasers and electro-optics in three different areas are presented.

INTECH
open science | open minds

InTech Europe
University Campus STeP Ri
Slavka Krautzeka 83/A
51000 Rijeka, Croatia
Phone: +385 (51) 770 447
Fax: +385 (51) 686 166
www.intechopen.com

InTech China
Unit 405, Office Block, Hotel Equatorial Shanghai
No.65, Yan An Road (West), Shanghai, 200040, China
中国上海市延安西路65号上海国际贵都大饭店办公楼405单元
Phone: +86-21-62489820
Fax: +86-21-62489821

IntechOpen